

A smooth, nonsingular, and faithful discretization scheme for polarizable continuum models: The switching/Gaussian approach

Adrian W. Lange and John M. Herbert^{a)}

Department of Chemistry, The Ohio State University, Columbus, Ohio 43210, USA

(Received 2 July 2010; accepted 15 October 2010; published online 28 December 2010)

Polarizable continuum models (PCMs) are a widely used family of implicit solvent models based on reaction-field theory and boundary-element discretization of the solute/continuum interface. An often overlooked aspect of these theories is that discretization of the interface typically does not afford a continuous potential energy surface for the solute. In addition, we show that discretization can lead to numerical singularities and violations of exact variational conditions. To fix these problems, we introduce the switching/Gaussian (SWIG) method, a discretization scheme that overcomes several longstanding problems with PCMs. Our approach generalizes a procedure introduced by York and Karplus [J. Phys. Chem. A **103**, 11060 (1999)], extending it beyond the conductor-like screening model. Comparison to other purportedly smooth PCM implementations reveals certain artifacts in these alternative approaches, which are avoided using the SWIG methodology. The versatility of our approach is demonstrated via geometry optimizations, vibrational frequency calculations, and molecular dynamics simulations, for solutes described using quantum mechanics and molecular mechanics. © 2010 American Institute of Physics. [doi:10.1063/1.3511297]

I. INTRODUCTION

This work focuses on a particular class of reaction-field models that are intended to describe a solute molecule immersed in a structureless dielectric medium. The solute has a charge distribution that might be calculated using quantum chemistry, or taken from a molecular mechanics (MM) force field, whereas the effects of the dielectric continuum, which is polarized by the solute's charge distribution, are represented by a charge density, $\sigma_{\text{pol}}(\vec{s})$, at the surface of a cavity that represents the solute/continuum boundary. Given the solute's charge density, $\rho_0(\vec{r})$, equations to define $\sigma_{\text{pol}}(\vec{s})$ are obtained by approximate solution of Poisson's equation, subject to cavity boundary conditions. Various levels of approximation have been reviewed recently,^{1,2} and Chipman²⁻⁴ has shown how all of these apparent surface charge (ASC) models can be cast within a common conceptual and computational framework. We adopt his notation as much as possible.

Nowadays, the ASC approach is virtually synonymous with the term polarizable continuum model (PCM), and encompasses such variants as the conductor-like model [C-PCM,⁵ also known as GCOSMO (Refs. 6 and 7)] as well as the integral equation formalism (IEF-PCM),⁸⁻¹⁰ which is also known by the acronym SS(V)PE (surface and simulation of volume polarization for electrostatics).³ The IEF-PCM and SS(V)PE methods are formally equivalent in their integral equation formulations.¹¹ The SS(V)PE approach provides an exact solution for the ASC arising from the charge density within the solute cavity, and an approximate solution for the volume polarization due to the "escaped charge," i.e., that part of ρ_0 that penetrates beyond the solute cavity.

For ASC models, one must specify a surface that defines the continuum boundary. When the solute is described us-

ing quantum chemistry, a conceptually appealing choice is to use an isodensity contour, $\rho_0(\vec{s}) = \text{constant}$,^{4,12} but this choice significantly complicates the formulation of analytic energy gradients. More often, the cavity is constructed from atom-centered (or functional-group-centered) spheres, whose radii might be related to atomic van der Waals (vdW) radii, or might simply be taken as empirical parameters in the model. With carefully parameterized united-atom radii, solvation free energies calculated using this simple prescription may actually be more accurate than those obtained from an isodensity construction.^{13,14}

The difficulty with all of these approaches, and the focus of the present work, lies in the discretization of the cavity surface into a finite set of surface elements, within which $\sigma_{\text{pol}}(\vec{s})$ is assumed to be constant. Thus, $\sigma_{\text{pol}}(\vec{s})$ is approximated using a finite set of surface grid points, \vec{s}_i , each with a surface area a_i , and $\sigma_{\text{pol}}(\vec{s})$ is replaced by a set of charges, q_i , located at these grid points. Given such a formulation, the potential energy surface of the solute molecule is inherently discontinuous, because the number of surface grid points changes discontinuously as a function of molecular geometry, with certain points disappearing into the solute cavity and others emerging from the cavity, onto the surface. These discontinuities hinder geometry optimizations, or prevent them from converging at all, introduce artifacts into vibrational frequency calculations, and pose problems for energy conservation in molecular dynamics simulations.¹⁵

Several schemes have been introduced to alleviate this problem,^{15,16,18-21} although none appears to be in widespread use at the present time. These methods differ in their details, but the unifying idea is to introduce a switching function that smoothly attenuates the contribution of a given surface element as it passes into the interior of the solute cavity. We have recently shown, however, that this is insufficient to produce a potential energy surface that is "smooth enough" for many

^{a)}Electronic mail: herbert@chemistry.ohio-state.edu.

chemical applications, even if it is rigorously smooth in the mathematical sense of possessing continuous derivatives.¹⁵ We find that the details of the potential surface are extremely sensitive to the balance between the switching function and the singular Coulomb potentials of the point charges that represent σ_{pol} ; naïve adoption of a switching function may lead to spurious oscillations in the energy or gradient.¹⁵

A more sophisticated smoothing approach is that pioneered by York and Karplus (YK),¹⁶ who represent σ_{pol} using spherical Gaussian charges, thereby eliminating the singularity in the Coulomb potential. The present work represents a generalization of the YK scheme that we call the switching/Gaussian (SWIG) method. Whereas YK consider only the conductor-like screening model (COSMO),¹⁷ our formulation is applicable to all ASC PCMs. A preliminary version of this work was reported in Ref. 15, and here we present a slightly modified version that is more faithful to the underlying integral equation theory. In addition, the present work provides additional details of the implementation, and a more thorough battery of tests and exemplary applications. Subsequent to our initial report,¹⁵ a similar approach was reported by Scalmani and Frisch,²¹ who refer to their implementation as the continuous surface charge (CSC) approach, a terminology that we shall adopt to refer to their implementation. The CSC method also attempts to generalize the YK approach, but differs in important details from the methodology presented here.

We will show that the SWIG approach possesses three critically important features: (i) it yields potential energy surfaces that are rigorously smooth, and also free of unwanted oscillations in the energy, the energy gradient, and the cavity surface area; (ii) the matrix formulation of SWIG is free of the singularities that pervade other smooth PCM formulations; and (iii) the SWIG discretization is faithful to the accuracy of the underlying integral equation theory, i.e., it does not greatly perturb the energetics. We believe that this is the first PCM discretization scheme to possess all three of these important properties.

The outline of this paper is as follows. In Sec. II, we review the fundamental reaction-field equations that lead to the general discretized PCM equations as formulated by Chipman.³ The SWIG formalism is presented in Sec. III, and in Sec. IV we analyze this approach in comparison with other discretization methods, pointing out several hitherto unnoticed problems with existing methods, including nonvariational solvation energies. In Sec. V, we present numerical results using both the C-PCM and SS(V)PE solvation models. In some cases the solute is described using an MM force field, while in other examples the solute is described using quantum mechanics, at the level of self-consistent field (SCF) theory. In Sec. VI we demonstrate the versatility and robustness of the SWIG discretization procedure with applications involving geometry optimization, calculation of vibrational spectra, and molecular dynamics simulations.

II. REACTION-FIELD THEORY

In this section, we present an overview of the PCM reaction-field formalism for the solute–continuum electro-

static interactions, then show how the resulting integral equations are discretized for numerical solution.

Nonelectrostatic interactions such as dispersion, repulsion, or cavitation are sometimes grafted onto ASC PCMs,¹ but will not be discussed here, except to note that the commonly used expressions for these interactions are functions of the total surface area of the cavity.^{22,23} As such, the continuity and smoothness of these nonelectrostatic interaction terms depends upon ensuring that the cavity surface area is a smooth function of the solute geometry. We have considered nonelectrostatic interactions in previous work,¹⁵ and found that the SWIG discretization suppresses spurious oscillations in the cavity surface area, which are sometimes observed using other smooth discretization schemes.

A. Electrostatic interactions

We begin by considering the electrostatic interactions of an arbitrary charge density embedded in a linear isotropic dielectric medium. We separate the total charge density into two components,

$$\rho_{\text{tot}}(\vec{r}) = \rho_0(\vec{r}) + \rho_{\text{pol}}(\vec{r}), \quad (2.1)$$

where ρ_0 is the solute’s charge density in the absence of the dielectric and ρ_{pol} is the density of bound charges that arises from polarization of the dielectric by the electric field due to ρ_0 . Similarly, the total electrostatic potential is decomposed according to

$$\phi_{\text{tot}}(\vec{r}) = \phi_0(\vec{r}) + \phi_{\text{pol}}(\vec{r}). \quad (2.2)$$

The quantity ϕ_{pol} is called the *reaction-field potential*, and originates with the charge distribution ρ_{pol} that is induced by the “reaction” of the dielectric in response to ϕ_0 , the field due to ρ_0 .²⁴ Such a response corresponds to displacement of bound charges within the dielectric, implying that a certain amount of work, w_{displ} , is required to induce ρ_{pol} .

The total electrostatic energy of the solute + continuum supersystem, W , is equal to the electrostatic interaction energy of the solute’s charge density with the polarized dielectric, plus the work required to displace the bound charges. We denote the latter quantity by w_{displ} , and therefore

$$W = w_{\text{displ}} + \frac{1}{2} \int \rho_{\text{tot}}(\vec{r}) \phi_{\text{tot}}(\vec{r}) d^3\vec{r}. \quad (2.3)$$

This energy can be separated into two components,

$$W = E_0 + E_{\text{pol}}, \quad (2.4)$$

where E_0 is the electrostatic self-energy associated with ρ_0 ,

$$E_0 = \frac{1}{2} \int \rho_0(\vec{r}) \phi_0(\vec{r}) d^3\vec{r}. \quad (2.5)$$

The other component of W is the *electrostatic solvation energy*,

$$\begin{aligned} E_{\text{pol}} = & \frac{1}{2} \int \rho_0(\vec{r}) \phi_{\text{pol}}(\vec{r}) d^3\vec{r} \\ & + \frac{1}{2} \int \rho_{\text{pol}}(\vec{r}) \phi_0(\vec{r}) d^3\vec{r} \\ & + \frac{1}{2} \int \rho_{\text{pol}}(\vec{r}) \phi_{\text{pol}}(\vec{r}) d^3\vec{r} + w_{\text{displ}}. \end{aligned} \quad (2.6)$$

The last two terms in this equation constitute the total work of inducing ρ_{pol} .

The appropriate microscopic expression for w_{displ} is not immediately obvious. However, by virtue of conservation of energy, the total work to induce ρ_{pol} must be equal and opposite to the energy gained by the dielectric in the interaction of ρ_{pol} with ϕ_0 :

$$\begin{aligned} & -\frac{1}{2} \int \rho_{\text{pol}}(\vec{r}) \phi_0(\vec{r}) d^3\vec{r} \\ & = \frac{1}{2} \int \rho_{\text{pol}}(\vec{r}) \phi_{\text{pol}}(\vec{r}) d^3\vec{r} + w_{\text{displ}}. \end{aligned} \quad (2.7)$$

This relation implies that w_{displ} can be cast in terms of the electrostatic interactions between the solute and polarization charges. In addition, it leads to the usual condensed expression for the electrostatic solvation energy,²⁵

$$E_{\text{pol}} = \frac{1}{2} \int \rho_0(\vec{r}) \phi_{\text{pol}}(\vec{r}) d^3\vec{r}. \quad (2.8)$$

This equation suggests that E_{pol} can be determined without explicit knowledge of w_{displ} , although we show in Appendix A that explicit expressions for w_{displ} can be derived for various PCMs.

In ASC PCM methods, it is assumed that ρ_0 occupies a cavity within the dielectric, and that ρ_{pol} can be recast into an *apparent* charge density, σ_{pol} , that resides entirely on the two-dimensional cavity surface. This surface charge density approximates the electrostatic potential due to ρ_{pol} :

$$\int \frac{\sigma_{\text{pol}}(\vec{s})}{|\vec{r} - \vec{s}|} d^2\vec{s} \approx \phi_{\text{pol}}(\vec{r}). \quad (2.9)$$

Given this approximation, and replacing $\rho_{\text{pol}}(\vec{r})$ with $\sigma_{\text{pol}}(\vec{s})\delta(\vec{r} - \vec{s})$ in Eq. (2.6), the electrostatic solvation energy can be rewritten entirely in terms of surface integrals,

$$\begin{aligned} E_{\text{pol}} & = w_{\text{displ}} + \int \sigma_{\text{pol}}(\vec{s}) \phi_0(\vec{s}) d^2\vec{s} \\ & + \frac{1}{2} \int \sigma_{\text{pol}}(\vec{s}) \hat{S} \sigma_{\text{pol}}(\vec{s}) d^2\vec{s}. \end{aligned} \quad (2.10)$$

The integral operator \hat{S} in this equation is defined such that $\hat{S} \sigma_{\text{pol}}(\vec{s}) = \phi_{\text{pol}}(\vec{s})$; see Appendix A for details. In deriving Eq. (2.10), we have used the identity

$$\int \rho_0(\vec{r}) \phi_{\text{pol}}(\vec{r}) d^3\vec{r} = \int \rho_{\text{pol}}(\vec{r}) \phi_0(\vec{r}) d^3\vec{r}, \quad (2.11)$$

which follows from the symmetry of the Coulomb interaction.

As an alternative to Eq. (2.10), E_{pol} can be written in the more traditional form

$$E_{\text{pol}} = \frac{1}{2} \int \sigma_{\text{pol}}(\vec{s}) \phi_0(\vec{s}) d^2\vec{s}, \quad (2.12)$$

using Eqs. (2.8) and (2.11). According to Eq. (2.12), calculation of E_{pol} is reduced to computation of σ_{pol} , which is the hallmark of ASC PCMs.

If ρ_0 is a polarizable charge density, as it is in quantum-mechanical (QM) calculations, then σ_{pol} may polarize and therefore modify ρ_0 , which in turn modifies σ_{pol} . In such cases, one must solve for E_0 and E_{pol} self-consistently,

by incorporating the polarization charge σ_{pol} into the SCF iterations.

B. Variational conditions

While Eq. (2.12) is convenient for computing the solvation energy, it is not very useful in deriving variational conditions for PCMs, because it masks the full functional dependence of E_{pol} [cf. Eq. (2.10)]. Here, we consider variation of Eq. (2.10).

In order for the total energy, W , to be a stationary point that is minimized with respect to variation of the surface charge density, the following relationship must hold:

$$\begin{aligned} 0 & = \frac{\delta W}{\delta \sigma_{\text{pol}}(\vec{s})} \\ & = \phi_0(\vec{s}) + \hat{S} \sigma_{\text{pol}}(\vec{s}) + \frac{\delta w_{\text{displ}}}{\delta \sigma_{\text{pol}}(\vec{s})}. \end{aligned} \quad (2.13)$$

To ensure that W is in fact *minimized* with respect to variation of σ_{pol} , we require that

$$\frac{\delta^2 W}{\delta \sigma_{\text{pol}}(\vec{s}) \delta \sigma_{\text{pol}}(\vec{s}')} = \hat{S} + \frac{\delta^2 w_{\text{displ}}}{\delta \sigma_{\text{pol}}(\vec{s}) \delta \sigma_{\text{pol}}(\vec{s}')} \quad (2.14)$$

is a positive-definite operator.

From Eq. (2.13), one obtains

$$-\phi_0(\vec{s}) = \hat{S} \sigma_{\text{pol}}(\vec{s}) + \frac{\delta w_{\text{displ}}}{\delta \sigma_{\text{pol}}(\vec{s})}, \quad (2.15)$$

which provides an equation relating ϕ_0 at the cavity surface to the apparent surface charge. As shown in Appendix A, Eq. (2.15) is a general equation that can be used to solve for σ_{pol} in PCM methods.

C. Discretization

The analytical formulation of reaction-field theory presented above can be solved exactly only in special cases, such as the Born ion model.²⁶ In order to apply reaction field theory to arbitrary charge densities and cavity shapes, the analytical formulation must be discretized and solved numerically. In this section we review how solute cavities are constructed and how the integral equations are transformed into finite-dimensional matrix equations.

1. Cavity shape

The first step in discretization is to define the shape of the cavity that defines the solute/continuum interface. Cavity shape is not unambiguous and certain shapes may be well-suited for some applications but not for others. Various approaches have been devised to construct cavities,¹ ranging from a single sphere that encompasses the entire solute, to a more realistic shape consisting of a union of spheres centered at each solute nucleus.

Typically, a set of atomic van der Waals radii, such as those deduced from crystallographic data by Bondi,²⁷ is used to define the spheres for each solute atom, although united-atom approaches have also been proposed.¹³ A surface composed of such spheres is called a vdW surface. The

vdW surface may exhibit crevices where finite-size solvent molecules should not be able to penetrate, hence the radii of the spheres are often augmented by adding a solvent probe radius to the vdW surface, resulting in a so-called solvent accessible surface (SAS).¹ Alternatively, the vdW radii might simply be scaled by a factor, typically 1.2,^{17,28} to mimic the same effect. Another common choice is the solvent excluding surface (SES), also known as a Connolly surface,²⁹ which smooths over the cusps of intersecting spheres in the vdW or SAS surface, by adding additional surface points. It has been noted,²¹ however, that certain algorithms for constructing the SES are inherently discontinuous, owing to the introduction of extra surface points. For this reason, we consider only SAS and vdW surfaces.

2. Cavity surface grid

With a cavity shape in hand, the next step is to divide the continuous surface into a grid of surface elements centered at points \vec{s}_i , with corresponding surface areas a_i . The most commonly used prescriptions are the Geometria Polihedro (GEPOL) algorithm³⁰ and Lebedev quadrature.³¹ GEPOL uses a regular 60-sided polyhedron to approximate a sphere, with surface elements that are triangles with areas $\tilde{a}_i = 4\pi R^2/60$, for a sphere of radius R . (More advanced extensions of the GEPOL grid have also been used.³²) The geometric gradients of \tilde{a}_i with respect to the nuclear coordinates are quite complicated,³² however, and we therefore use Lebedev grids exclusively, in order to simplify the formulation of analytic energy gradients. Lebedev grids, which are used almost universally to perform the numerical integration steps in density-functional theory calculations, are spherical grids having octahedral symmetry, with quadrature weights w_i that are formulated to provide exact integrals for spherical harmonics, Y_{lm} , up to a given value of l .³¹ When a Lebedev grid is used to discretize a sphere of radius R , the individual surface elements have areas

$$\tilde{a}_i = w_i R^2. \quad (2.16)$$

The trouble with these discretization procedures is that surface elements will emerge from and/or vanish into the interior of the cavity as the solute nuclei move. As a result, both E_{pol} and the cavity surface area are discontinuous functions of the coordinates of the nuclei. Historically, this issue has been largely ignored, although several groups have recently worked on methods designed to ameliorate the discontinuities.^{15,16,19–21} Common to all of these methods is the introduction of a geometry-dependent switching function, F_i , for each surface element, such that the area of the i th surface element is

$$a_i = \tilde{a}_i F_i, \quad (2.17)$$

where $0 \leq F_i \leq 1$.

3. Electrostatic energy

The fundamental assumption of the discretization procedure is that the electrostatic environment (ϕ_0 , σ_{pol} , etc.) varies

TABLE I. Definitions of the matrices in Eq. (2.18), for the PCMs considered here. The matrix \mathbf{A} is diagonal and consists of the surface element areas, a_i , while the matrices \mathbf{S} and \mathbf{D} are defined in the text. The quantity ε represents the dielectric constant of the medium.

Method	Matrix \mathbf{K}	Matrix \mathbf{R}
C-PCM	\mathbf{S}	$-\left(\frac{\varepsilon-1}{\varepsilon}\right)\mathbf{I}$
SS(V)PE	$\mathbf{S} - \left(\frac{\varepsilon-1}{\varepsilon+1}\right)\left(\frac{1}{4\pi}\right)(\mathbf{DAS} + \mathbf{SAD}^\dagger)$	$-\left(\frac{\varepsilon-1}{\varepsilon+1}\right)\mathbf{I} - \left(\frac{1}{2\pi}\right)\mathbf{DA}$

slowly within each surface element,⁴ so that $\sigma_{\text{pol}}(\vec{s})$ may be assumed to be constant over a given area, a_i . Naturally, this approximation improves as the density of the surface grid increases and the individual areas become small. Discretization converts the surface charge density, $\sigma_{\text{pol}}(\vec{s})$, into a vector \mathbf{q} , whose elements q_i are the surface charges for the various surface area elements. In most PCM implementations, q_i is treated as a point charge located at \vec{s}_i . Likewise, $\phi_0(\vec{s})$ is given by a vector \mathbf{v} , where $v_i = \phi_0(\vec{s}_i)$.

Chipman and Dupuis⁴ have shown that discretization of the cavity surface results in a set of linear equations,

$$\mathbf{Kq} = \mathbf{Rv}, \quad (2.18)$$

that determine the vector \mathbf{q} . The matrices \mathbf{K} and \mathbf{R} depend upon the particular PCM, and are written in terms of two other matrices, \mathbf{S} and \mathbf{D} , that are discussed in Sec. III A and in Appendix A. The forms of \mathbf{K} and \mathbf{R} for C-PCM and SS(V)PE are listed in Table I.

Some remarks about terminology should be made at this point. Although the IEF-PCM and SS(V)PE models are formally equivalent, at the level of integral equations,¹¹ discretization fails to preserve the equality $\mathbf{DAS} = \mathbf{SAD}^\dagger$ [cf. Eq. (A3) in Appendix A].³ As such, one can envisage various asymmetric forms of \mathbf{K} , or a symmetrized version that employs $(\mathbf{DAS} + \mathbf{SAD}^\dagger)/2$. Authors who use the term ‘‘IEF-PCM’’ have generally employed an asymmetric form of \mathbf{K} ,^{8–10} whereas Chipman uses the notation ‘‘SS(V)PE’’ for the symmetric variant.³ In the present work, we use only the symmetric form of \mathbf{K} , hence we refer to this method as SS(V)PE. (In future work, we plan to compare the symmetric and asymmetric forms of \mathbf{K} .) For brevity, we use the term C-PCM to refer to the conductor-like model, noting that it is completely equivalent to the model known as GCOSMO.

Returning to Eq. (2.18), we can express this equation in the alternative form

$$\mathbf{q} = \mathbf{Qv}, \quad (2.19)$$

where $\mathbf{Q} = \mathbf{K}^{-1}\mathbf{R}$ is often called the *response matrix*, since the action of \mathbf{Q} on \mathbf{v} affords the surface charges \mathbf{q} that are induced in response to the electrostatic potential, \mathbf{v} . Formally, computation of \mathbf{q} requires inversion of \mathbf{K} , although iterative algorithms that avoid matrix diagonalization have been developed.³³ Upon discretizing the integral that defines E_{pol} in Eq. (2.12), one can express the electrostatic solvation energy in a variety of equivalent forms:

$$E_{\text{pol}} = \frac{1}{2}\mathbf{q}^\dagger\mathbf{v} = \frac{1}{2}\mathbf{q}^\dagger\mathbf{Q}^{-1}\mathbf{q} = \frac{1}{2}\mathbf{v}^\dagger\mathbf{Q}\mathbf{v}. \quad (2.20)$$

The total energy is then

$$W = E_0 + \frac{1}{2} \mathbf{q}^\dagger \mathbf{v}. \quad (2.21)$$

The variational principle analogous to Eq. (2.13) is

$$0 = \frac{\partial W}{\partial \mathbf{q}^\dagger} = \mathbf{v} - \mathbf{Q}^{-1} \mathbf{q}, \quad (2.22)$$

which is equivalent to Eq. (2.19). However, the derivation of Eq. (2.22) assumes that $\mathbf{Q}^\dagger = \mathbf{Q}$, which is true within C-PCM but not for SS(V)PE. Fortunately, E_{pol} is invariant to the following symmetrization:

$$E_{\text{pol}} = \frac{1}{4} \mathbf{v}^\dagger [\mathbf{K}^{-1} \mathbf{R} + \mathbf{R}^\dagger (\mathbf{K}^\dagger)^{-1}] \mathbf{v}. \quad (2.23)$$

As such, we may replace \mathbf{Q} in the energy expressions with a symmetric matrix

$$\tilde{\mathbf{Q}} = \frac{1}{2} (\mathbf{Q} + \mathbf{Q}^\dagger). \quad (2.24)$$

This symmetrization is crucial for efficient evaluation of energy gradients.

To ensure that W is minimized by the induced surface charges \mathbf{q} , let us compute the second variation of W with respect to \mathbf{q} . Using Eq. (2.22), one obtains

$$\frac{\partial^2 W}{\partial \mathbf{q}^\dagger \mathbf{q}} = -\mathbf{Q}^{-1}. \quad (2.25)$$

It follows that in order for W to be a local minimum, the matrix $-\mathbf{Q}^{-1}$ must be positive-definite, hence \mathbf{Q} must be negative-definite. If so, then it follows from Eq. (2.20) that $E_{\text{pol}} < 0$ for any \mathbf{v} and any \mathbf{q} . The physical implication of this result is that the reaction field always lowers the total energy. We will revisit this important point in Sec. IV, in regard to the choice of matrix elements for the smooth version of SS(V)PE.

4. Electrostatic gradients

PCM analytic energy gradients have been reported previously,^{34–38} but we briefly summarize the formalism here, in order to make contact with the reaction-field formalism presented above. Differentiating the total energy with respect to a perturbation, x , and using the notation $W^x = \partial W / \partial x$, we have

$$W^x = E_0^x + E_{\text{pol}}^x. \quad (2.26)$$

The quantity E_0^x is simply the gas-phase gradient of the solute, computed using a density matrix that is converged in the presence of the reaction field. The polarization energy gradient is

$$E_{\text{pol}}^x = \frac{1}{2} [(\mathbf{v}^\dagger)^x \mathbf{Q} \mathbf{v} + \mathbf{v}^\dagger \mathbf{Q}^x \mathbf{v} + \mathbf{v}^\dagger \mathbf{Q} \mathbf{v}^x]. \quad (2.27)$$

The first and third terms on the right are equivalent if \mathbf{Q} is symmetric, but as indicated above, we may replace \mathbf{Q} in this expression with the symmetric matrix $\tilde{\mathbf{Q}}$ from Eq. (2.24). This is required in order to avoid the appearance of the density matrix derivative, the calculation of which would require solution of coupled-perturbed equations.³⁹ To avoid this costly endeavor, it is necessary to perform the symmetrization of \mathbf{Q} in Eq. (2.24) or, alternatively, to calculate two sets of charges, $\mathbf{q}' = \mathbf{Q} \mathbf{v}$ and $\mathbf{q}'' = \mathbf{Q}^\dagger \mathbf{v}$. Combining the two sets as

TABLE II. Gradients of the matrices in Table I, for the two PCMs considered here. For brevity, we have defined $\mathbf{M}^x = \mathbf{D}^x \mathbf{A} \mathbf{S} + \mathbf{D} \mathbf{A}^x \mathbf{S} + \mathbf{D} \mathbf{A} \mathbf{S}^x$.

Method	Matrix \mathbf{K}^x	Matrix \mathbf{R}^x
C-PCM	\mathbf{S}^x	0
SS(V)PE	$\mathbf{S}^x - \left(\frac{\epsilon-1}{\epsilon+1}\right) \left(\frac{1}{4\pi}\right) [\mathbf{M}^x + (\mathbf{M}^x)^\dagger]$	$\left(\frac{\epsilon-1}{\epsilon+1}\right) \left(\frac{1}{2\pi}\right) (\mathbf{D}^x \mathbf{A} + \mathbf{D} \mathbf{A}^x)$

$\mathbf{q} = \frac{1}{2}(\mathbf{q}' + \mathbf{q}'')$ is equivalent to performing the symmetrization of Eq. (2.24).

Using Eq. (2.23) we can rewrite E_{pol}^x as

$$E_{\text{pol}}^x = \frac{1}{2} \mathbf{v}^\dagger (\mathbf{K}^{-1} \mathbf{R})^x \mathbf{v} + \mathbf{q} \mathbf{v}^x. \quad (2.28)$$

The physical interpretation of this equation is that the surface charges experience the full electric field of the solute but only half that of the surface charge density, a consequence of the work required to induce the cavity surface charge. The second term on the right in Eq. (2.28) is straightforward to compute, since \mathbf{q} must be computed anyway in order to obtain E_{pol} , and \mathbf{v}^x is simply the electric field at a given surface grid point, a standard quantity at both MM and QM levels of theory. The remaining term in E_{pol}^x can be rearranged and simplified into a general form for all PCMs:

$$\mathbf{v}^\dagger (\mathbf{K}^{-1} \mathbf{R})^x \mathbf{v} = \mathbf{v}^\dagger \mathbf{K}^{-1} (\mathbf{R}^x - \mathbf{K}^x \mathbf{K}^{-1} \mathbf{R}) \mathbf{v}. \quad (2.29)$$

Further manipulation of this term requires us to choose a particular PCM. Expressions for \mathbf{K}^x and \mathbf{R}^x for both C-PCM and SS(V)PE are provided in Table II.

III. THE SWITCHING/GAUSSIAN METHOD FOR CAVITY DISCRETIZATION

We now come to the main topic of this work: the switching/Gaussian (SWG) cavity discretization procedure.

A. Surface charge representation and matrix elements

An important distinction between various cavity discretization methods is the manner in which the surface charge density, $\sigma_{\text{pol}}(\vec{s})$, is represented, leading to different definitions of the matrices \mathbf{S} and \mathbf{D} upon which \mathbf{K} and \mathbf{R} depend (see Table I). The matrices \mathbf{S} and \mathbf{D} are the discrete forms of certain integral operators, \hat{S} and \hat{D} , that act on $\sigma_{\text{pol}}(\vec{s})$,^{1,2,40} and which are briefly reviewed in Appendix A. In discrete form, the action of \mathbf{S} on \mathbf{q} produces the electrostatic potential due to \mathbf{q} , evaluated at the set of points $\{\vec{s}_i\}$. The action of \mathbf{D} on \mathbf{q} produces the surface-dipole (double-layer) potential,³ again evaluated at the points $\{\vec{s}_i\}$. The action of \mathbf{D}^\dagger on \mathbf{q} affords the surface normal component of the electric field. Multiplying by the area a_i for each surface point provides an approximate normal electric field over the i th surface element, and a compact notation is obtained by introducing a diagonal matrix, \mathbf{A} , with elements $A_{ij} = a_i \delta_{ij}$ (see Table I).

The matrix elements of \mathbf{S} and \mathbf{D} are derived from the Coulomb operator between surface charges, and thus depend upon how this surface charge is represented. The most

common choice is to use point charges q_i located at the discretization points \vec{s}_i , but following YK,¹⁶ we will represent $\sigma_{\text{pol}}(\vec{s})$ using spherical Gaussians centered at the points \vec{s}_i :

$$g_i(\vec{r}) = q_i (\zeta_i^2/\pi)^{3/2} \exp(-\zeta_i^2 |\vec{r} - \vec{s}_i|^2). \quad (3.1)$$

The amplitude q_i in this equation is precisely the charge that appears in the vector \mathbf{q} , and the exponent ζ_i is allowed to depend upon the surface area of the i th surface element. Specifically, if we denote the radius of the I th atomic sphere by R_I , then for a Lebedev quadrature point $i \in I$ located on this sphere, the Gaussian exponent, ζ_i , is chosen to be¹⁶

$$\zeta_i = \frac{\zeta}{R_I \sqrt{w_i}}. \quad (3.2)$$

Here, ζ is a width parameter that is optimized, for each particular Lebedev grid, in order to reproduce the Born solvation energy of a conductor and a uniform surface charge distribution.^{16,41} (Numerical values of ζ are taken from Ref. 16.)

The Gaussian charge basis eliminates the Coulomb singularity present in point charge interactions, so that the surface charge interactions remain finite at all geometries. This is important, as we have found that the use of a switching function can exacerbate problems with singularities in the PCM equations, by allowing surface grid points to approach more closely than they would in standard (discontinuous) discretization schemes.¹⁵

Having selected a representation for the surface charge, the off-diagonal matrix elements of \mathbf{S} and \mathbf{D} follow quite readily. The off-diagonal element S_{ij} is simply the Coulomb interaction between g_i and g_j , which can be evaluated analytically. The result is

$$S_{ij} = \frac{\text{erf}(\zeta_{ij} r_{ij})}{r_{ij}}, \quad (3.3)$$

where $r_{ij} = |\vec{r}_i - \vec{r}_j|$ and $\zeta_{ij} = \zeta_i \zeta_j / (\zeta_i^2 + \zeta_j^2)^{1/2}$. The off-diagonal element D_{ij} is related to S_{ij} according to the relation¹

$$D_{ij} = \vec{n}_j \cdot \frac{\partial S_{ij}}{\partial \vec{r}_j}, \quad (3.4)$$

where \vec{n}_j is the outward pointing unit vector normal to the cavity surface, at the point \vec{s}_j . Using Eqs. (3.3) and (3.4), we obtain

$$D_{ij} = \left(\text{erf}(\zeta_{ij} r_{ij}) - \frac{2\zeta_{ij} r_{ij}}{\sqrt{\pi}} e^{-\zeta_{ij}^2 r_{ij}^2} \right) \frac{\vec{n}_j \cdot \vec{r}_{ij}}{r_{ij}^3}, \quad (3.5)$$

where $\vec{r}_{ij} = \vec{r}_i - \vec{r}_j$.

The diagonal matrix elements S_{ii} and D_{ii} , which are termed the *self-potential* and the *self-field* interactions, respectively,²¹ are not straightforward to define because they involve Coulomb interactions within a discretized surface element. At the same time, these self-interactions turn out to be critically important to obtaining a smooth potential energy surface as well as solvation energies that are faithful to the integral equation PCM theory. Because Gaussian charges eliminate the singularity in the Coulomb potential, an obvious choice for the self-potential interaction is based upon the observation that

$$\lim_{r_{ij} \rightarrow 0} \frac{\text{erf}(\zeta_{ii} r_{ij})}{r_{ij}} = \zeta_i \sqrt{2/\pi}. \quad (3.6)$$

We use this limit to define S_{ii} . To ensure smoothness, however, S_{ii} must be scaled by the inverse of the switching function F_i , consistent with the original YK prescription.¹⁶ Thus, we define

$$S_{ii} = \frac{\zeta_i \sqrt{2/\pi}}{F_i}. \quad (3.7)$$

The precise nature of the switching function is discussed in Sec. III B. For now, it suffices to note that the presence of F_i in the denominator of S_{ii} ensures continuity of the potential surface, as shown in Appendix B.

The quantity D_{ii} is related to the interaction of $\sigma_{\text{pol}}(\vec{s}_i)$ with its own normal electric field component, and the product $D_{ii} a_i$ gives the total interaction over the entire area a_i . In our previous work,¹⁵ we noted that $\lim_{r_{ij} \rightarrow 0} D_{ij} = 0$, and used this as justification to set $D_{ii} = 0$. While this choice is certainly valid in the limit that $a_i \rightarrow 0$, in practice it tends to degrade the accuracy of solvation energies,³⁷ and our subsequent experience has shown that smooth PCMs with $D_{ii} = 0$ cannot reproduce Born ion solvation energies across a range of dielectric constants. In the present work, we define

$$D_{ii} = -\frac{\zeta_i \sqrt{2/\pi}}{2R_I}, \quad (3.8)$$

where R_I is the radius of the atomic sphere on which the point \vec{s}_i resides. This choice is based upon the definition $D_{ii} = S_{ii}/2R_I$ from Ref. 9. We find that this approach does reproduce Born-ion solvation energies

Having defined \mathbf{S} and \mathbf{D} , the analytic gradients for SWIG can be derived by taking the gradient of the matrix elements with respect to the M th solute nucleus. For S_{ij} with $i \neq j$, we obtain

$$\hat{\nabla}_M S_{ij} = -\left(\text{erf}(\zeta_{ij} r_{ij}) - \frac{2\zeta_{ij} r_{ij}}{\sqrt{\pi}} e^{-\zeta_{ij}^2 r_{ij}^2} \right) \frac{\hat{\nabla}_M r_{ij}}{r_{ij}^2}, \quad (3.9)$$

whereas

$$\hat{\nabla}_M S_{ii} = -\frac{\zeta_i \sqrt{2/\pi}}{F_i^2} \hat{\nabla}_M F_i. \quad (3.10)$$

The switching function gradient, $\hat{\nabla}_M F_i$, is given in Appendix C. For the diagonal elements of \mathbf{D} , we have

$$\hat{\nabla}_M D_{ii} = 0, \quad (3.11)$$

whereas for $i \neq j$ we obtain

$$\begin{aligned} \hat{\nabla}_M D_{ij} = & \left(\frac{4r_{ij}^2 \zeta_i^3}{\sqrt{\pi}} e^{-r_{ij}^2 \zeta_i^2} \right) \frac{\vec{n}_j \cdot \vec{r}_{ij}}{r_{ij}^3} \hat{\nabla}_M r_{ij} \\ & - \left(\text{erf}(\zeta_{ij} r_{ij}) - \frac{2\zeta_{ij} r_{ij}}{\sqrt{\pi}} e^{-\zeta_{ij}^2 r_{ij}^2} \right) \\ & \times \left(\frac{\vec{n}_j (\delta_{jM} - \delta_{iM})}{r_{ij}^3} + \frac{3\vec{n}_j \cdot \vec{r}_{ij}}{r_{ij}^4} \hat{\nabla}_M r_{ij} \right). \end{aligned} \quad (3.12)$$

An equivalent form of Eq. (3.12) was given in Ref. 15.

The quantity $\hat{\nabla}_M r_{ij}$, which appears in both Eqs. (3.9) and (3.12), vanishes unless either $i \in M$ or $j \in M$. We can express this derivative as

$$\hat{\nabla}_M r_{ij} = \frac{\vec{r}_i - \vec{r}_j}{r_{ij}} (\delta_{iM} - \delta_{jM}), \quad (3.13)$$

where $\delta_{iM} = 1$ if $i \in M$, else $\delta_{iM} = 0$.

B. Switching functions

We have already introduced a dimensionless switching function, F_i , for the i th discretization point, although its precise form has not yet been specified. The function F_i should smoothly attenuate the i th surface point's contribution to the solvation energy, as \vec{s}_i passes into or out of the cavity. The cavity consists of a union of spheres centered at points $\{\vec{r}_J\}$, and a reasonable *ansatz* for F_i is a product of elementary switching functions,^{15,16}

$$F_i = \prod_{J, i \notin J}^{\text{atoms}} f(\vec{s}_i, \vec{r}_J). \quad (3.14)$$

The elementary switching functions, $f(\vec{s}_i, \vec{r}_J)$, should vary smoothly and monotonically between zero and one. Equation (3.14) ensures that F_i depends upon the nuclear coordinates of the entire solute molecule, and will be zero if even a single $f(\vec{s}_i, \vec{r}_J) = 0$. In practice, we set $f(\vec{s}_i, \vec{r}_J)$ to zero whenever this function drops below 10^{-8} . In our experience, this does not produce any numerically detectable discontinuities.

There are probably many different choices for the function f that would work in this context; we will describe two choices that we have found to work well in practice. The first of these, originally proposed by YK,¹⁶ is based upon definition of a switching region around each atomic sphere. Using $R_{\text{sw},J}$ to denote the width of the switching region around the J th atom, the inner and outer boundaries of the switching region for atom J are defined by radii

$$R_{\text{in},J} = R_J - \alpha_J R_{\text{sw},J} \quad (3.15)$$

and

$$R_{\text{out},J} = R_J + (1 - \alpha_J) R_{\text{sw},J}, \quad (3.16)$$

respectively, where α_J is an adjustable parameter ($0 < \alpha_J < 1$). The definitions of the parameters α_J and $R_{\text{sw},J}$ depend upon R_J and also the number of Lebedev grid points used to discretize the J th sphere; these definitions, which we take from Ref. 16, are provided in the supporting information.⁴²

The extent to which the i th grid point penetrates into the switching region surrounding the J th sphere is measured using the dimensionless quantity

$$d_{iJ} = \frac{|\vec{s}_i - \vec{r}_J| - R_{\text{in},J}}{R_{\text{sw},J}}. \quad (3.17)$$

The elementary switching function used by YK is then given by

$$f(\vec{s}_i, \vec{r}_J) = h(d_{iJ}), \quad (3.18)$$

where

$$h(x) = \begin{cases} 0 & x < 0 \\ x^3(10 - 15x + x^2) & 0 \leq x \leq 1 \\ 1 & x > 1 \end{cases}. \quad (3.19)$$

In later work, York and co-workers⁴³ replaced F_i in Eq. (3.14) with F_i^p , where the exponent p was taken to be an additional adjustable parameter. However, we have demonstrated that values of $p \neq 1$ can lead to unwanted oscillations in the energy gradient,¹⁵ so we take $p = 1$ throughout this work.

The switching function defined above is certainly not unique, and even within this *ansatz*, parameters such as $R_{\text{sw},J}$ and α_J are not unique either. York and co-workers^{16,43} have presented some arguments in favor of simple formulas that define these parameters, and we have adopted these definitions because they produce good results in a variety of tests. It is likely that a somewhat different switching function could be found that, in conjunction with Gaussian surface charges, also affords good results.

To this end, we have explored some alternative switching functions, to make comparison and perhaps to diminish some of the arbitrariness in this aspect of the SWIG method. One such alternative is to exploit the spatial extent of the spherical Gaussian charges to determine the penetration of a surface element into the cavity. The idea is to compute the fraction of the Gaussian charge distribution g_i that exists inside of the J th sphere. Restricting ourselves to one dimension for simplicity, we obtain the resulting elementary switching function

$$f(\vec{s}_i, \vec{r}_J) = 1 - \frac{1}{2} \{ \text{erf}[\zeta_i(R_J - r_{iJ})] + \text{erf}[\zeta_i(R_J + r_{iJ})] \}, \quad (3.20)$$

where R_J is the radius of the J th sphere and $r_{iJ} = |\vec{s}_i - \vec{r}_J|$. The term in curly braces measures how much normalized charge density exists inside the J th sphere. Thus, $f(\vec{s}_i, \vec{r}_J) = 0$ when the i th Gaussian is contained entirely within the J th sphere. To distinguish between the elementary switching function in Eq. (3.18), versus that defined in Eq. (3.20), we henceforth refer to the latter approach as the improved SWIG (ISWIG) method, whereas "SWIG" will imply that the YK switching function in Eq. (3.18) is used. In all other respects, the two methods are identical.

A potential advantage of ISWIG is that it accounts for differences in the relative extents of the Gaussian charges, whereas the SWIG approach uses a switching function that is independent of the Gaussian exponents, ζ_i . Using ISWIG, a Gaussian charge with a small width will be rapidly attenuated as it penetrates into an atomic sphere, whereas SWIG will attenuate this charge more slowly, if the switching region is large relative to the Gaussian charge width. ISWIG should also avoid situations in which a broad Gaussian charge is centered just outside of a switching region, with a substantial amount of its charge distribution inside the cavity, yet is fully switched on. On the other hand, the SWIG switching function is somewhat more efficient computationally, since its switching regions extend over a fairly narrow region around each atomic sphere. In numerical tests performed so far, both SWIG and ISWIG afford similar results.

IV. COMPARISON TO OTHER DISCRETIZATION METHODS

We next compare and contrast our discretization methods to two others that have recently been proposed as solutions to the PCM discontinuity problem, namely, the fixed points with variable areas (FIXPVA) method of Su and Li,²⁰ and the continuous surface charge (CSC) method of Scalmani and Frisch.²¹ All three of these methods claim to yield smooth potential energy surfaces through the use of a switching function, yet there exist subtle but important differences between them.

A. Continuity

Matrix elements for the FIXPVA and CSC methods are given in Table III. Of these two approaches, CSC is more similar to SWIG, and in fact uses the same off-diagonal elements S_{ij} and D_{ij} , in conjunction with Gaussian charges, and the same switching function as that defined in Eq. (3.18). The FIXPVA approach uses point charges, and this choice necessitates the use of an alternative switching function,²⁰ as close approach of these point charges must be avoided.

The switching function does not appear explicitly in the matrix elements S_{ii} for the FIXPVA and CSC methods, but is instead folded into the areas a_i . However, we can cast the SWIG expression for S_{ii} [Eq. (3.7)] into something that more closely resembles the expressions in Table III by using Eq. (3.2) to relate ζ_i to $a_i = w_i R_I^2 F_i$:

$$S_{ii} = \zeta \sqrt{\frac{2}{\pi a_i F_i}}. \quad (4.1)$$

Thus, SWIG, CSC, and FIXPVA all attenuate surface points via the diagonal of \mathbf{S} , and in Appendix B we show that this is sufficient to obtain a smooth potential energy surface. As such, all three methods afford potential energy surfaces that are smooth, in the mathematical sense.

TABLE III. Matrix elements of \mathbf{S} and \mathbf{D} for the FIXPVA and CSC methods. In Ref. 21, the CSC matrix elements are defined for spheres of unit radius, but we have generalized them here to arbitrary areas, a_i . We have also generalized the FIXPVA approach of Ref. 20 for use with SS(V)PE, as described in the text. In the expressions for S_{ii} , R_I is the radius of the I th sphere ($i \in I$), and the constant C_S is a self-energy factor that depends upon the choice of surface grid: $C_S = 1.0694$ for GEPOL grids (Ref. 37) and $C_S = 1.104$ for Lebedev grids (Ref. 44).

Matrix element	FIXPVA value	CSC value
S_{ij}	$1/r_{ij}$	$\text{erf}(\zeta_{ij} r_{ij})/r_{ij}$
S_{ii}	$C_S \sqrt{\frac{4\pi}{a_i}}$	$\left(4\pi R_I - \sum_{j \neq i} S_{ij} a_j\right) / a_i$
D_{ij}	$\vec{n}_j \cdot \vec{r}_{ij} / r_{ij}^3$	$\left(\text{erf}(\zeta_{ij} r_{ij}) - \frac{2\zeta_{ij} r_{ij}}{\sqrt{\pi}} e^{-\zeta_{ij}^2 r_{ij}^2}\right) \frac{\vec{n}_j \cdot \vec{r}_{ij}}{r_{ij}^3}$
D_{ii}	$-\left(2\pi + \sum_{j \neq i} D_{ij} a_j\right) / a_i$	$-\left(2\pi + \sum_{j \neq i} D_{ij} a_j\right) / a_i$

B. Sum rules

As compared to the off-diagonal elements of \mathbf{S} and \mathbf{D} , formulation of the self-energy and self-field within a given surface element, and therefore the diagonal matrix elements S_{ii} and D_{ii} , is less straightforward. Traditionally, D_{ii} has been defined using a sum rule,

$$D_{ii} = -\frac{1}{a_i} \left(2\pi + \sum_{j \neq i} D_{ij} a_j\right), \quad (4.2)$$

which avoids the need to determine D_{ii} by ill-conditioned numerical integration over the i th surface element, and furthermore provides more accurate energetics than simply setting $D_{ii} = 0$.^{37,45} This sum rule was originally derived by Purisima and Nilar,⁴⁶ starting from the discretized expression for \hat{D} ,

$$\sum_j \int \frac{(\vec{r}_j - \vec{r}_i) \cdot \vec{n}_j}{r_{ij}^3} d^2 \vec{s}_j = -\sum_j D_{ij} a_j. \quad (4.3)$$

These authors recognized that the integrals appearing in Eq. (4.3) could be rewritten as a solid angle integral over each surface element, from which it follows that

$$-\sum_j D_{ij} a_j = \sum_j \int d\Omega_j = 2\pi. \quad (4.4)$$

Here, $d\Omega_j$ is the solid angle subtended by the j th surface element, from the vantage point \vec{s}_i on the cavity surface.

Equation (4.2) is used to define D_{ii} in the CSC method.²¹ In addition, we have used this sum rule to extend the FIXPVA discretization method to the SS(V)PE approach (see Table III), whereas FIXPVA discretization was previously introduced only in the context of C-PCM.²⁰

For S_{ii} , the FIXPVA method employs the widely used formula $S_{ii} = C_S (4\pi/a_i)^{1/2}$, where C_S is a numerical constant representing the average value of the Coulomb self-repulsion integral over surface elements of various sizes.^{17,37,44} The CSC method, in contrast, uses a sum rule

$$S_{ii} = \frac{1}{a_i} \left(4\pi R_I - \sum_{j \neq i} S_{ij} a_j\right) \quad (4.5)$$

that is derived²¹ by minimizing an approximate functional for the Born solvation energy of a spherical ion in a conductor, with respect to the Coulomb interaction between surface charges. Only the CSC approach uses the sum rule in Eq. (4.5).

Because the surface charge is assumed to be constant over the area a_i , the self-interaction over a_i is strictly repulsive. Therefore, the quantities $q_i^2 S_{ii}$ and $-q_i^2 D_{ii}$ must both be positive. (The matrix \mathbf{D} is traditionally defined such that $-D_{ii}$ is the actual contribution of the self-field to the PCM equations.) In the SWIG approach developed here, these matrix elements are defined such that $S_{ii} > 0$ and $D_{ii} < 0$ by construction, and $S_{ii} > 0$ is also guaranteed in the FIXPVA approach. When sum rules are used to define these matrix elements, however, there is no guarantee that the correct sign is obtained. (In earlier work,¹⁵ this problem led us to set $D_{ii} = 0$.) For the CSC discretization scheme, which uses sum rules to

define both S_{ii} and D_{ii} , this is potentially a problem for all variants of PCM theory, including the C-PCM method where the \mathbf{D} matrix is absent.

From Eq. (4.2) we see that $D_{ii} > 0$ if $\sum_{j \neq i} D_{ij} a_j < -2\pi$, for some particular cavity geometry. This condition occurs readily when point charges are used in conjunction with a switching function, due to close approach of point charges leading to some $D_{ij} \ll 0$. Even when Gaussians are employed, however, we have found that the requirement $D_{ii} < 0$ is regularly violated for any solute cavity consisting of more than one sphere.

Clearly, Eq. (4.2) is no longer exact within these smooth PCM approaches. One reason is that the relationship between the integral in Eq. (4.3) and the solid angle integral in Eq. (4.4) is derived based on a pointwise discretization, whereas our surface elements are spherical Gaussians. More importantly, Eq. (4.4) is valid only if the surface elements and vantage points all reside on a closed surface, but when switching functions are used, some of the “surface” points \vec{s}_i actually reside *inside* the cavity. For vantage points inside of the cavity, the total solid angle subtended by the surface is $\sum_j \int d\Omega_j = 4\pi$.⁴⁶ Thus, if \vec{s}_i lies inside of the cavity surface, we should expect that

$$-\sum_{j \neq i} D_{ij} a_j \approx 4\pi, \quad (4.6)$$

which we have verified in numerical calculations. It follows from Eqs. (4.2) and (4.6) that $D_{ii} a_i \approx 2\pi$ in this case, in violation of the condition $D_{ii} < 0$. We have not inspected the sum rule for S_{ii} , Eq. (4.5), but it may be subject to similar issues.

Breakdown of the sum rules has serious consequences. In our initial report of SWIG,¹⁵ we mentioned the sum rule issue for D_{ii} and pointed out that it can compromise the positive-definiteness of the matrix \mathbf{K} , causing numerical instabilities. We have since determined that loss of positive-definiteness of \mathbf{K} is not the fundamental origin of these instabilities. Instead, they arise due to violation of the negative-definiteness of \mathbf{Q} , resulting in nonvariational surface charge densities and singularities in E_{pol} . A numerical exploration of this issue is presented in Sec. V A.

V. NUMERICAL TESTS

In this section, we present numerical comparisons of various discretization methods, along with numerical tests of convergence with respect to the Lebedev grid density. We have implemented the SWIG, ISWIG, and FIXPVA discretization schemes within a locally modified version of Q-Chem.⁴⁷ To make contact with the CSC approach,²¹ we have also implemented a variant of SWIG that uses the CSC (sum rule) definition of D_{ii} in Eq. (4.2), as opposed the SWIG definition in Eq. (3.8). We refer to this modified approach as “subSWIG.”

Except for one set of calculations in Sec. V B, where spherical solute cavities are used, all calculations use cavities constructed from a union of atomic spheres. For QM solutes, we use Bondi’s values for the vdW radii,²⁷ except for hydrogen where a vdW radius of 1.1 Å is used.⁴⁸ The vdW radii are then scaled by a factor of 1.2 for use in cavity construc-

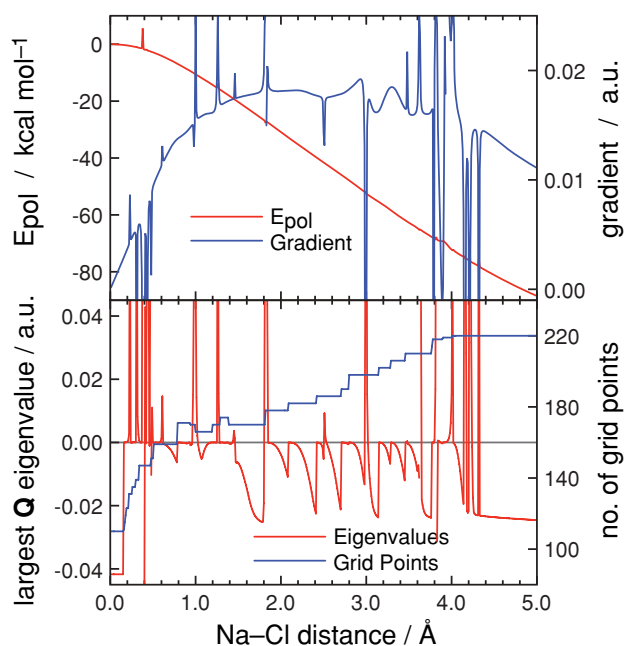


FIG. 1. NaCl dissociation in water ($\epsilon = 78.39$), computed at the AMBER99/SS(V)PE level using the “subSWIG” discretization scheme in which D_{ii} is defined using the sum rule in Eq. (4.2). Panel (a) plots the solvation energy, E_{pol} , and its gradient with respect to Cl displacement, while panel (b) plots the largest eigenvalue of \mathbf{Q} , along with the number of surface grid points for which $F_i > 10^{-8}$. Data points were calculated at 0.01 Å intervals. For clarity, the vertical scale has been truncated in both panels, i.e., some of the sharp spikes are off of the scale that is used.

tion. For MM solutes, unscaled Lennard-Jones radii from the AMBER99 force field⁴⁹ are used to construct the cavity.

A. Bond breaking

Dissociation of NaCl in water provides an illustrative example of the consequences that accompany breakdown of the sum rule that is used to define D_{ii} in the CSC/subSWIG approach. Here, we compute various quantities along the Na–Cl dissociation coordinate, using the AMBER99 force field for the NaCl solute,⁵⁰ and the SS(V)PE solvation model for the aqueous solvent.

Figure 1 shows some results using subSWIG discretization. A single, sharp spike in E_{pol} (for which $E_{\text{pol}} > 0$) can be seen in the solvation energy curve, while the gradient of E_{pol} is rapidly oscillatory. Figure 1(b) shows that rapid oscillations in the gradient are correlated with geometries for which the \mathbf{Q} matrix exhibits one or more positive eigenvalues. In contrast, SWIG discretization (Fig. 2) produces comparatively minor oscillations in the gradient, and \mathbf{Q} remains rigorously negative-definite at all solute geometries.

The failure of subSWIG to preserve negative-definiteness of \mathbf{Q} opens the possibility of nonvariational solvation energies ($E_{\text{pol}} > 0$), although in Fig. 1(a) we see only a single instance where $E_{\text{pol}} > 0$, and it occurs at an unrealistically short Na–Cl distance, where one sphere completely envelops the other. However, the benign appearance of Fig. 1(a) turns out to be an artifact of the relatively large spacing (0.01 Å) between the data points. If we take much smaller steps, as in Fig. 3, we discover sharp spikes in the solvation energy at

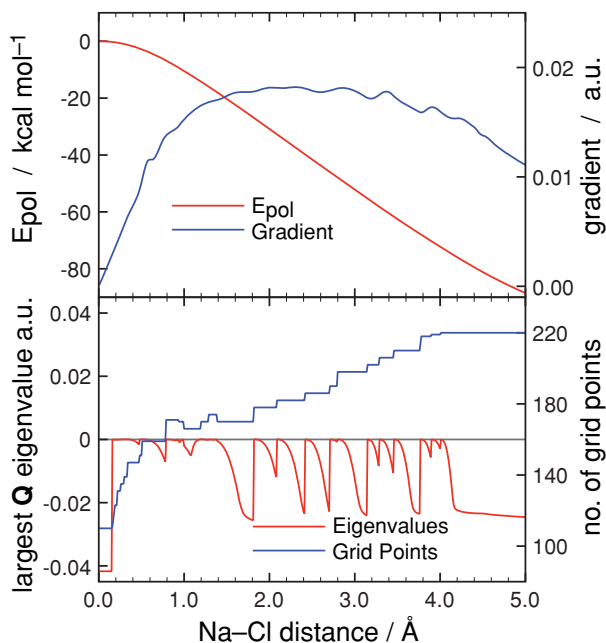


FIG. 2. NaCl dissociation in water ($\epsilon = 78.39$), computed at the AMBER99/SS(V)PE level using the SWIG discretization scheme. Panel (a) plots the solvation energy, E_{pol} , and its gradient with respect to Cl displacement, while panel (b) plots the largest eigenvalue of \mathbf{Q} , along with the number of surface grid points for which $F_i > 10^{-8}$. Data points were calculated at 0.01 Å intervals.

other internuclear distances, which are correlated in each case with positive eigenvalues of \mathbf{Q} . These singularities exist despite the fact that subSWIG employs both a switching function and Gaussian surface charges, and is equivalent to SWIG except that it uses a sum rule to define D_{ii} . The regions where $E_{\text{pol}} > 0$ are highly localized, so it is not surprising that the energy curve in Fig. 1(a), where the data points are 0.01 Å apart, fortuitously avoids these anomalies. Nevertheless, we will see that these singularities are encountered in realistic calculations on polyatomic solutes, and that they pose real problems.

Examining the largest eigenvalue of \mathbf{Q} in the case of SWIG discretization [Fig. 2(b)], one might worry about what appear to be sharp jumps in this eigenvalue, but in fact these oscillations are perfectly natural. As shown in Appendix B, the switching function causes \mathbf{Q} to exhibit a null space corresponding to those surface elements for which $F_i = 0$, so that the largest (i.e., least negative) eigenvalue of \mathbf{Q} must approach zero as any $F_i \rightarrow 0$. Figure 2(b) shows that rapid oscillations in this eigenvalue are indeed correlated with changes in the number of grid points for which F_i exceeds our drop tolerance of 10^{-8} .

B. Solvation energies

Certain PCM theories and cavity shapes may be more or less accurate than others for predicting solvation free energies, but ideally we would like to separate this aspect of the model from the smoothing procedure, so that the smoothed model is faithful to the underlying PCM and does not significantly perturb solvation energies, relative to those obtained using es-

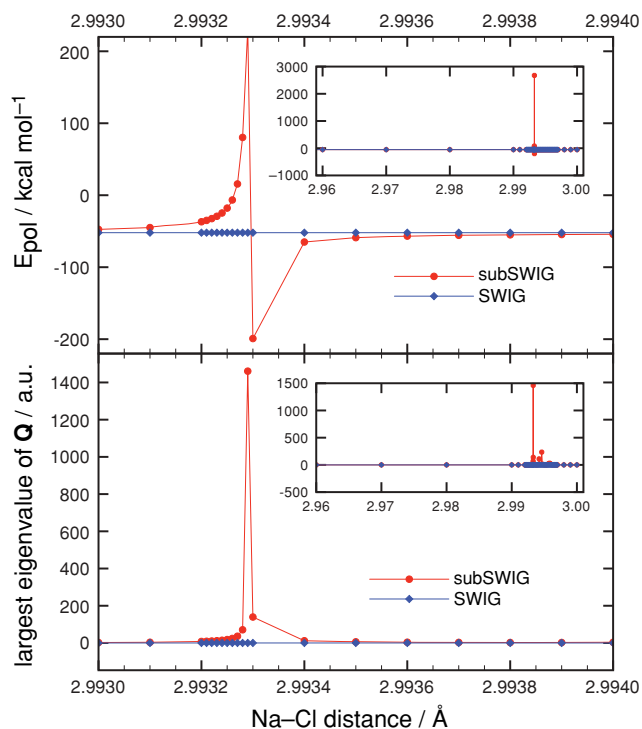


FIG. 3. Solvation energy, E_{pol} , and eigenvalues of \mathbf{Q} , near a singular point of the subSWIG potential energy surface for NaCl dissociation. (Data points are calculated every 10^{-4} Å.) The inset shows a larger range of internuclear distances, and suggests that singularities may go unnoticed unless the spacing between data points is extremely small.

established discretization schemes. As a representative example of the latter, we choose the variable tesserae number (VTN) discretization method,¹⁹ which uses point charges and does not employ a switching function. The VTN scheme was developed as a “less discontinuous” discretization method, and serves as a baseline against which to compare the SWIG, CSC, and FIXPVA methods. The VTN method uses the same matrix elements as FIXPVA (see Table III), but does not scale the areas with a switching function. Instead, F_i in Eq. (2.17) is replaced with a delta function, according to whether the i th grid point is inside of the cavity or not. VTN calculations are therefore subject to Coulomb singularities as well as discontinuities.

As a first set of tests, we examine the molecules H_2O , CH_3CONH_2 , NO^+ , and CN^- , which were previously used by Chipman² to test his isodensity implementation of the SS(V)PE model. We do not employ an isodensity cavity construction, but instead place each molecule inside of a spherical cavity centered at the molecule’s center of mass, and discretized using 1202 Lebedev grid points. The radius of this cavity is selected in order to replicate the solvation energies reported by Chipman,² computed in our case using SS(V)PE[VTN]. Using a spherical cavity allows us to sidestep issues of continuity and smoothness in this set of tests, and thereby examine the extent to which the Gaussian surface charges perturb solvation energies, as compared to the baseline VTN discretization. (Note that the switching function is irrelevant here, since the cavity consists of a single sphere.)

TABLE IV. Comparison of solvation energies (in kcal/mol), using a solute cavity consisting of a single sphere whose radius is adjusted in order to reproduce the solvation energies reported in Ref. 2, where an isodensity contour was used to define the cavity surface.

		$\epsilon = 78.304$ (water)			
Theory	Method	H ₂ O	CH ₃ CONH ₂	NO ⁺	CN ⁻
C-PCM	VTN	-8.69	-10.91	-88.47	-67.32
	SWIG	-8.69	-10.93	-88.49	-67.30
SS(V)PE	VTN	-8.58	-10.81	-88.47	-67.31
	SWIG	-8.62	-10.84	-88.48	-67.29
		$\epsilon = 2.379$ (toluene)			
Theory	Method	H ₂ O	CH ₃ CONH ₂	NO ⁺	CN ⁻
C-PCM	VTN	-4.90	-6.43	-52.30	-39.56
	SWIG	-4.90	-6.45	-52.31	-39.55
SS(V)PE	VTN	-3.92	-5.01	-52.21	-39.35
	SWIG	-3.92	-5.02	-52.22	-39.34

Solvation energies for the aforementioned molecules are reported in Table IV, where they were computed using the same procedure as in Ref. 2. Specifically, each molecule was optimized in the gas phase at the Hartree–Fock (HF) level to obtain the gas-phase energy, E_{gas} . The 6-31G** basis set was used for all molecules except CN⁻, for which we used the 6-31+G* basis. Solvation energies, $E_{\text{solv}} = W - E_{\text{gas}}$, were then computed at the gas-phase geometry, where W [Eq. (2.3)] is the solution-phase energy for some particular choice of PCM and discretization method. We performed these calculations in both a high-dielectric solvent (water) and a low-dielectric solvent (toluene). The results in Table IV demonstrate that SWIG discretization reproduces VTN energies to within 0.04 kcal/mol, in either solvent, using both the C-PCM and SS(V)PE solvation models. We take these results to indicate that Gaussian smoothing of the surface charges has a negligible effect on the energetics of the underlying PCM.

To ascertain the effects of the switching function on E_{solv} , we need to use nonspherical cavities, so we repeated the calculations on H₂O, CH₃CONH₂, NO⁺, and CN⁻ using a vdW cavity constructed from a union of atomic spheres, as described above. Each sphere was discretized using a 1202-point Lebedev grid, discarding any points for which $F_i < 10^{-8}$. Solvation energies are reported in Table V for the VTN, SWIG, ISWIG, and subSWIG discretization methods.

These various discretization schemes afford very similar solvation energies at the C-PCM level, but results computed using SS(V)PE vary over a somewhat wider range. In particular, the SWIG and subSWIG discretization schemes differ by as much as 1.3 kcal/mol for NO⁺ and CN⁻ in water, the cases where the solvation energy is largest. VTN solvation energies are quite close to those obtained using other discretization methods, except in the case of CH₃CONH₂ in water, where discrepancies as large as 1.6 kcal/mol are observed.

While it is not completely clear what is the most accurate value of E_{solv} , we are inclined to prefer the SWIG and ISWIG results, which agree with the other discretization schemes at the C-PCM level, where the \mathbf{D} matrix is absent, yet are free of singularities at the SS(V)PE level. The SWIG and ISWIG solvation energies in Table V differ from one another by no

TABLE V. Comparison of solvation energies (in kcal/mol) using a vdW cavity composed of atomic spheres. Note that SWIG and subSWIG discretization procedures are equivalent in the case of C-PCM.

		$\epsilon = 78.304$ (water)			
Theory	Method	H ₂ O	CH ₃ CONH ₂	NO ⁺	CN ⁻
C-PCM	VTN	-6.94	-10.05	-81.33	-69.73
	SWIG	-6.93	-10.04	-81.28	-69.69
	ISWIG	-6.93	-10.05	-81.28	-69.70
SS(V)PE	VTN	-6.89	-11.38	-80.69	-69.62
	subSWIG	-6.89	-9.99	-81.26	-69.69
	SWIG	-6.82	-9.81	-79.96	-68.86
	ISWIG	-6.86	-9.90	-80.55	-69.27
		$\epsilon = 2.379$ (toluene)			
Theory	Method	H ₂ O	CH ₃ CONH ₂	NO ⁺	CN ⁻
C-PCM	VTN	-3.92	-5.49	-47.74	-40.78
	SWIG	-3.91	-5.49	-47.71	-40.76
	ISWIG	-3.91	-5.49	-47.71	-40.76
SS(V)PE	VTN	-3.26	-4.49	-47.32	-40.71
	subSWIG	-3.25	-4.70	-47.39	-40.68
	SWIG	-3.24	-4.68	-47.02	-40.43
	ISWIG	-3.25	-4.70	-47.20	-40.56

more than 0.6 kcal/mol, which is comparable to (or smaller than) the intrinsic error in solvation energies computed using models of this type.⁵¹

C. Discretization errors

In most finite-element methods, energy is not rigorously rotationally invariant. When Poisson’s equation is integrated on a three-dimensional grid, however, our experience suggests that violations of rotational invariance are quite small.⁵² For the ASC PCMs considered here, rotational invariance is not preserved because each octahedral Lebedev grid is constructed in the laboratory frame, then translated to the atomic center in question. Although the energy will be rotationally invariant in the limit of an infinitely dense discretization grid, it is desirable to know what is the smallest number of Lebedev grid points that affords tolerable errors.

We assess rotational invariance for the SWIG discretization scheme using the 20 standard amino acids as a data set. We choose these molecules because (i) MM parameters are readily available for them; (ii) their side chains exhibit a variety of chemical properties (polar and nonpolar, charged and neutral, etc.); and (iii) proteins are often investigated with implicit solvent models. The geometries of the amino acids were generated, in their zwitterionic forms, using the TINKER program,⁵⁴ and were not further optimized. For each amino acid, we calculated the energy at each of ten randomly generated rotations of the TINKER structure, and quantified the rotational invariance according to the quantity

$$\Delta_{\text{rot}} = \frac{1}{20} \sum_A^{\text{amino acids}} \left[\frac{1}{10} \sum_{i=1}^{10} (W_{A,i} - \bar{W}_A)^2 \right]^{1/2}, \quad (5.1)$$

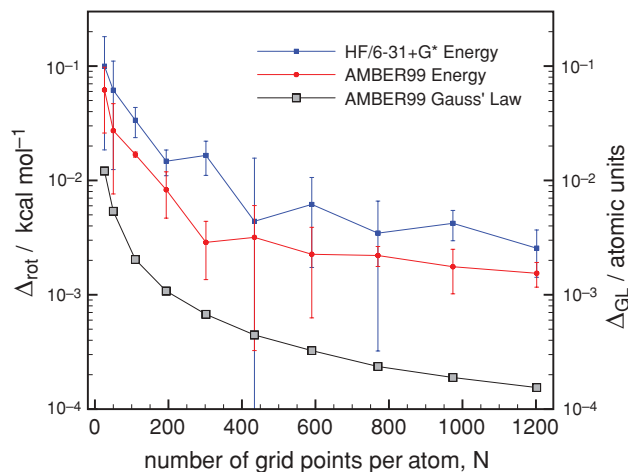


FIG. 4. Rotational variance, Δ_{rot} , and Gauss' Law error, Δ_{GL} , as a function of the number of grid points per atom, for a set of 20 amino acids in water ($\epsilon = 78.39$). Error bars represent one standard deviation about the mean. For clarity, the error bars are omitted for Δ_{GL} , but can be found in the supporting information (Ref. 42).

where $W_{A,i}$ represents the energy of the i th orientation of amino acid A , and \overline{W}_A is the average over the ten values of $W_{A,i}$.

Figure 4 plots Δ_{rot} versus the number of Lebedev grid points per atomic sphere, for both QM (HF/6-31+G*) and MM (AMBER99) solutes, at the C-PCM[SWIG] level. Even for the sparsest grid that we tested (26 grid points per atomic sphere), $\Delta_{\text{rot}} < 0.1$ kcal/mol. The error is solute-dependent, of course, but combined with small rotational errors observed by YK for a different set of solutes,¹⁶ these results indicate that errors in rotational invariance are essentially negligible when Lebedev grids are used.

We also calculate the error in Gauss' Law for this same data set. Restricting our attention to the AMBER99 case, for which ρ_0 is contained entirely within the cavity, we can write Gauss' Law as

$$\int \sigma_{\text{pol}}(\vec{s}) d^2\vec{s} = -\left(\frac{\epsilon - 1}{\epsilon}\right) \int \rho_0(\vec{r}) d^3\vec{r}. \quad (5.2)$$

The deviation from this exact equality can be quantified as

$$\Delta_{\text{GL}} = \frac{1}{20} \sum_A^{\text{amino acids}} \left\{ \frac{1}{10} \sum_{i=1}^{10} \left[Q_{A,i}^{\text{surf}} + \left(\frac{\epsilon - 1}{\epsilon}\right) Q_A \right]^2 \right\}^{1/2}, \quad (5.3)$$

where $Q_{A,i}^{\text{surf}}$ is the total surface charge on amino acid A in its i th orientation, and Q_A net charge on this amino acid. The dependence of Δ_{GL} on the number of grid points is shown in Fig. 4, and as with Δ_{rot} , we find that Δ_{GL} is reasonably small, even for sparse grids.

To investigate the convergence of the total energy, W , with respect to the Lebedev grid density, we used this same set of amino acids (but only one orientation for each), and examined the energy differences $W_N - W_{1202}$, where the subscript indicates the number of grid points per atomic sphere. These differences are plotted, as a function of N , in Fig. 5, for both AMBER99 and HF/6-31+G* solutes. (In the latter

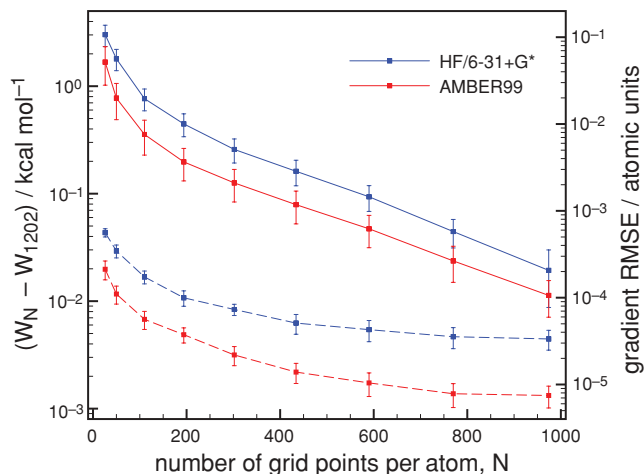


FIG. 5. Plots of the C-PCM[SWIG] discretization error, $W_N - W_{1202}$, (solid lines) and the RMSE of the gradient (broken lines), as a function of the number of Lebedev grid points per atomic sphere. Data points represent averages over the set of 20 amino acids in water ($\epsilon = 78.39$), with error bars representing one standard deviation on either side of the mean.

case, the discretization errors that we observe using atom-centered Lebedev grids are comparable, as a function of N , to those obtained using an isodensity cavity discretized with a single-center Lebedev grid.²) The energy discretization error is significant for the smallest grids but is reduced to less than 0.5 kcal/mol, on average, for $N = 110$ (AMBER99) or $N = 194$ (HF/6-31+G*). That the HF calculations are more sensitive to N likely reflects the more complicated topography of the electrostatic potential, relative to that generated by a collection of point charges.

Figure 5 also plots the root mean square error (RMSE) in the energy gradient, as compared to the result obtained using 1202 Lebedev points per atomic sphere. When N is small, the RMSE is comparable in magnitude to the gradient itself ($\sim 10^{-2}$ a.u. for the unoptimized amino acid structures). However, for $N = 110$ (AMBER99) and $N = 194$ (HF/6-31+G*), the RMSE in the gradient drops below 10^{-4} a.u.

Numerical data for the convergence tests in the section can be found, in tabular form, in the supporting information.⁴²

VI. SAMPLE APPLICATIONS

In this section we use SWIG in several applications that demand smooth potential energy surfaces, and compare the results to those obtained using FIXPVA and subSWIG discretization. All calculations reported in the section assume that the solute and solvent remain in equilibrium at all times; see Ref. 1 for a discussion of nonequilibrium solvation. Solute cavities in these applications are constructed as described in Sec. V.

A. Geometry optimization and vibrational frequency analysis

In our initial report of the SWIG method,¹⁵ we demonstrated that certain discretization schemes give rise to spurious harmonic frequencies, when computed by finite difference of

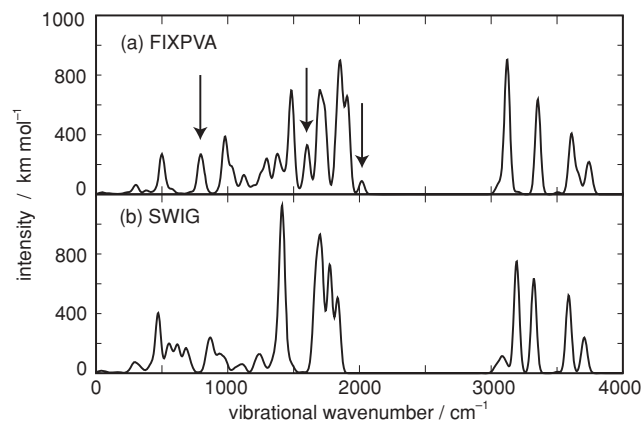


FIG. 6. Harmonic vibrational spectrum of Arg-Asp in water ($\epsilon = 78.39$), computed by finite difference of analytic energy gradients at the B3LYP/6-31G*/C-PCM level, with either (a) FIXPVA or (b) SWIG discretization. Stick spectra were convolved with 20 cm^{-1} Gaussians. Arrows indicate peaks in the FIXPVA spectrum that have no obvious analogues in the SWIG spectrum at nearby frequencies.

analytic energy gradients, as is often the required when the solute is described using a correlated wavefunction. On the other hand, the “solute” in the example of Ref. 15 consisted of adenine plus 52 explicit MM water molecules, and is arguably not representative of most applications of PCMs. Here, we consider some more pedestrian examples.

1. Comparison to FIXPVA

As a first application, we compute harmonic vibrational frequencies for the dipeptide arginine–aspartate (Arg-Asp), in aqueous solution at the B3LYP/6-31G* level, using C-PCM in conjunction with either SWIG or FIXPVA discretization. The initial structure of the dipeptide, in its zwitterionic form, was generated using the TINKER program,⁵⁴ and subsequently optimized in the gas phase. The gas-phase structure was then optimized with C-PCM[SWIG] and, separately, with C-PCM[FIXPVA]. (Atomic spheres were discretized using 110 Lebedev grid points.) Unfortunately, these two solution-phase optimizations converged to quite different structures, making for an unfair comparison. Thus, the FIXPVA optimization was restarted from the SWIG optimized structure, and ultimately similar optimized geometries were obtained from both methods. Harmonic frequencies were then computed by finite difference of analytic energy gradients, with a step size of 10^{-3} \AA . The resulting spectra are shown in Fig. 6.

Because the SWIG and FIXPVA discretizations afford somewhat different potential energy surfaces, one should not expect these methods to yield identical vibrational spectra. Nevertheless, it is worrisome that there are a few peaks present in the FIXPVA spectrum, largely involving N–H and C–H stretching modes, that have no obvious analogues in the SWIG spectrum. Although these peaks do appear in an appropriate spectral region for such modes (unlike some of the spurious peaks in the adenine–water example from Ref. 15), upon closer examination we find that the vibrations in question are

associated with finite-difference steps that rapidly turn on or off certain surface elements, causing a sharp change in the FIXPVA energy and gradient and a large perturbation in the harmonic frequency. On the other hand, the SWIG spectrum appears to be free of peaks associated with dramatic changes in the cavity surface.

The FIXPVA potential energy surface is rigorously smooth, mathematically speaking, so discontinuities cannot explain spurious peaks in the vibrational spectrum. Instead, the rapid fluctuations in the gradient that give rise to these peaks result from the fact that the FIXPVA switching function attenuates the surface elements much more rapidly than the switching functions used in the SWIG and ISWIG methods. Rapid switching is necessary within the FIXPVA approach, in order to avoid singularities arising from close approach of surface point charges. However, this rapid scaling of the surface element areas can lead to “holes” in the cavity surface, in regions of high surface grid density.¹⁵ These holes lead to a poor representation of $\sigma_{\text{pol}}(\vec{s})$ and an underestimate of the cavity surface area.^{15,20} Although the FIXPVA switching function prevents r_{ij} from every being *exactly* zero (by attenuating the surface elements in question as $r_{ij} \rightarrow 0$), the delicate balance between the switching function and the singular Coulomb potential is sufficient to cause unwanted oscillations in energy and gradient, even for the relatively small perturbations used in finite-difference calculations. (Such oscillations can also lead to the appearance of spurious maxima and/or minima in the potential energy surface.¹⁵)

Although stable geometry optimizations in large molecules have been reported using FIXPVA,²⁰ these calculations were carried out using a GEPOL cavity surface, and are not directly comparable to what is reported here. It is possible that Lebedev grids exacerbate the difficulties with FIXPVA, because the Lebedev grid points are distributed less uniformly than are the GEPOL tesserae, and may therefore be closer together in some cases. In the present work, we took parameters for the FIXPVA switching function from Ref. 20, where they were determined for use with GEPOL. Reparameterization for Lebedev grids might mitigate some of the problems that we observe using FIXPVA, but will not eliminate the delicate balance between the switching function and the singular Coulomb potential that requires the use of a rapidly varying switching function. We avoid this requirement here, by means of Gaussian surface charges.

2. Comparison to CSC/subswig

Strong Coulomb interactions are not the only possible cause of spurious lines in vibrational spectra. To illustrate, we compute the harmonic vibrational spectrum of a glycerol molecule in liquid glycerol solution ($\epsilon = 42.7$) at the HF/6-31G*/SS(V)PE level using both the SWIG and subSWIG discretizations. (Recall that these methods are the same, except that subSWIG uses the CSC sum rule to define the D_{ii} matrix elements.) Details of the calculations were the same as for the Arg-Asp calculations described above, except that in this case, both discretization schemes afford essentially identical

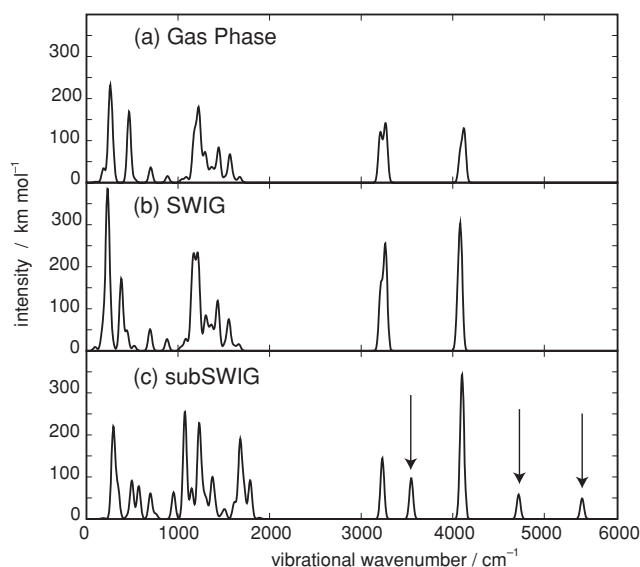


FIG. 7. Harmonic vibrational spectra of glycerol computed at the HF/6-31G* level in (a) the gas phase; (b) liquid glycerol ($\epsilon = 42.7$), described at the SS(V)PE[SWIG] level; and (c) liquid glycerol, described at the SS(V)PE[subSWIG] level. Stick spectra were convolved with 20 cm^{-1} Gaussians. Arrows indicate spurious peaks in the subSWIG spectrum.

solution-phase geometries, and this geometry is very close to that obtained in the gas phase. Vibrational spectra are depicted in Fig. 7.

Although the gas-phase spectrum and SS(V)PE[SWIG] spectrum are similar (as one might expect, given that the PCM alters the geometry very little), the SS(V)PE[subSWIG] spectrum exhibits peaks that are clearly absent in these other spectra. Two of these features, which are associated with C–H stretching modes, have frequencies above 4700 cm^{-1} , and are clearly artifacts. These artifacts arise as a consequence of violations in the variational principle that result when D_{ii} is defined using a sum rule. It is worth noting that not all of the peaks are affected by this problem; the O–H stretching peak around 4000 cm^{-1} , for example, is quite similar in all three spectra shown in Fig. 7.

B. Molecular dynamics

A molecular dynamics (MD) calculation is an especially stringent test of PCM cavity discretization, because such a calculation may explore a broad swath of the solute’s potential energy surface, and because conservation of energy places demands on how rapidly the energy may change as a function of solute geometry. Here, we report MD simulations in a PCM, using both QM and MM descriptions of the solute.

1. Molecular mechanics

We propagated molecular dynamics for a single-stranded DNA oligomer, d(GACT), using the AMBER99 force field to describe the DNA and the C-PCM model to describe the aqueous solvent ($\epsilon = 78.39$). A time step of 1.0 fs was used, with initial velocities sampled from a Boltzmann distribution at $T = 300 \text{ K}$.

Figure 8 compares the energy fluctuations observed using SWIG and FIXPVA discretization, as well as those from a gas-phase MD simulation of the same solute. The d(GACT) molecule is fairly flexible, and undergoes considerable geometric rearrangement over 10 ps, substantially altering the cavity shape. The FIXPVA approach is unable to cope with these changes, and exhibits a catastrophic failure to conserve energy, with two jumps of $\gtrsim 10 \text{ kcal/mol}$ within the first 3 ps of simulation. Eventually, one of these jumps simply crashes the simulation, due to an overflow error in the atomic velocities. As in the case of FIXPVA geometry optimizations, these abrupt changes in energy originate in the too-close approach of surface charges as grid points vanish into, or emerge from, the interior of the cavity. The SWIG discretization, on the other hand, exhibits energy fluctuations of only $\sim 0.2 \text{ kcal/mol}$ over the entire 10 ps of the simulation, which is comparable to what is observed in the gas phase.

2. Ab initio MD

As a second MD example, we performed an *ab initio* MD simulation on glycine in water, with the solute described at the PBE0/6-31+G* level, using the SS(V)PE model. We compare the ISWIG discretization approach to “subiSWIG,” which substitutes the sum rule in Eq. (4.2) as a definition of D_{ii} . The simulations begin at the gas-phase optimized geometry and use initial velocities corresponding to the zero-point energy of the gas phase vibrational modes, with a time step of 0.97 fs. Energy fluctuations are shown in Fig. 9. Within the first 15 fs, the subiSWIG simulation encounters a singularity, leading to a jump in the energy of nearly 100 kcal/mol. After several more large jumps, the simulation eventually reaches a geometry for which the SCF procedure fails to converge. Three separate attempts with subiSWIG were made, using slightly different initial conditions, but each suffered the same fate. In contrast, the ISWIG discretization conserves energy just as well as the gas phase simulation, and is stable through at least 5 ps of simulation.

In aqueous solution, the lowest-energy tautomer of glycine is the zwitterion $^+\text{NH}_3\text{CH}_2\text{CO}_2^-$, whereas the neutral form $[\text{NH}_2\text{CH}_2\text{C}(\text{O})\text{OH}]$ is $\sim 11 \text{ kcal/mol}$ higher in energy, but in the gas phase the neutral form is more stable by $\sim 18 \text{ kcal/mol}$.^{55,56} Our SS(V)PE[ISWIG] simulations bear this out; starting from the gas-phase geometry, in which the carboxylic acid moiety is protonated, the molecule eventually undergoes an intramolecular proton transfer to form the zwitterion, a process that is not observed in the gas-phase MD simulation. Figure 10 shows that the solvation energy changes smoothly as this proton transfer occurs.

VII. SUMMARY

This work introduces the Switching/Gaussian (SWIG) discretization method for apparent surface charge PCMs, which generalizes a method originally introduced by York and Karplus¹⁶ in the context of the conductor-like screening model. The approach developed here is applicable not only to C-PCM/GCOSMO calculations, but also to more

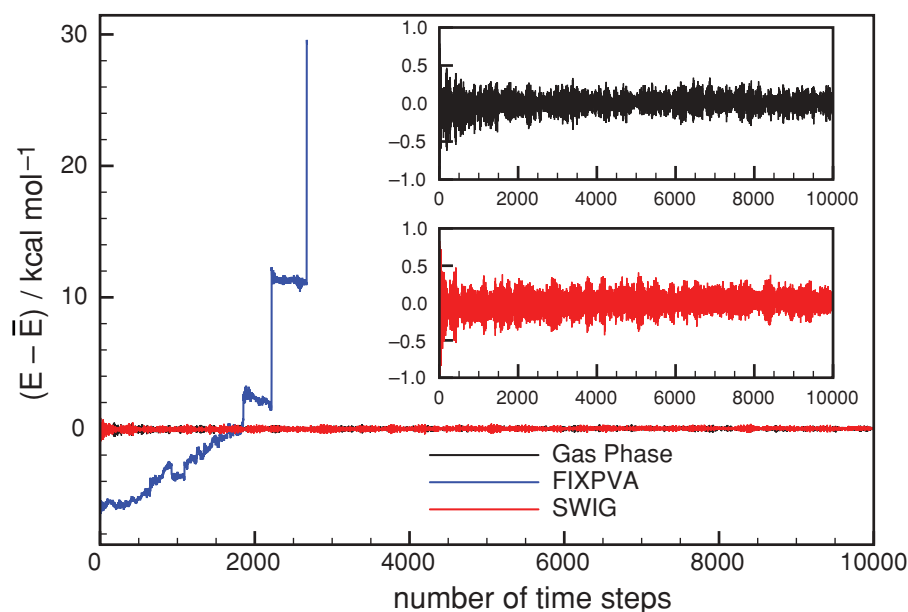


FIG. 8. Fluctuations in the energy during an MD simulation of single-stranded d(GACT) in water, described at the AMBER99/C-PCM level. The inset shows a close-up view of the energy fluctuations obtained in the gas phase and with C-PCM[SWIG]. The time step is 1.0 fs.

sophisticated PCMs such as SS(V)PE and IEF-PCM. Both QM and MM solutes are possible.

Comparison to other “smooth discretization” approaches reveals that while these alternative methods may afford potential energy surfaces that are rigorously smooth, in a mathematical sense, they suffer from Coulomb singularities when point charges are used to represent the surface charge. This problem can be eliminated by using spherical Gaussian functions to represent the surface charge, but in this case, the approximate nature of certain sum rules that are traditionally used in these models can lead to nonvariational singularities in the solvation energy.

The SWIG approach eliminates both of these problems, by using Gaussian surface charges but avoiding the use of sum rules to define the matrix elements of the PCM equations. The result is a method that affords smooth potential energy surfaces and is largely free of unwanted oscillations in the energy gradient, so that molecular dynamics simulations are stable and robust, and harmonic vibrational frequencies can safely be calculated by finite difference of analytic energy gradients. SWIG discretization also appears to be faithful to the energetics of the underlying integral-equation PCM. As such, there seems to be no reason *not* to use this discretization method for all PCM calculations.

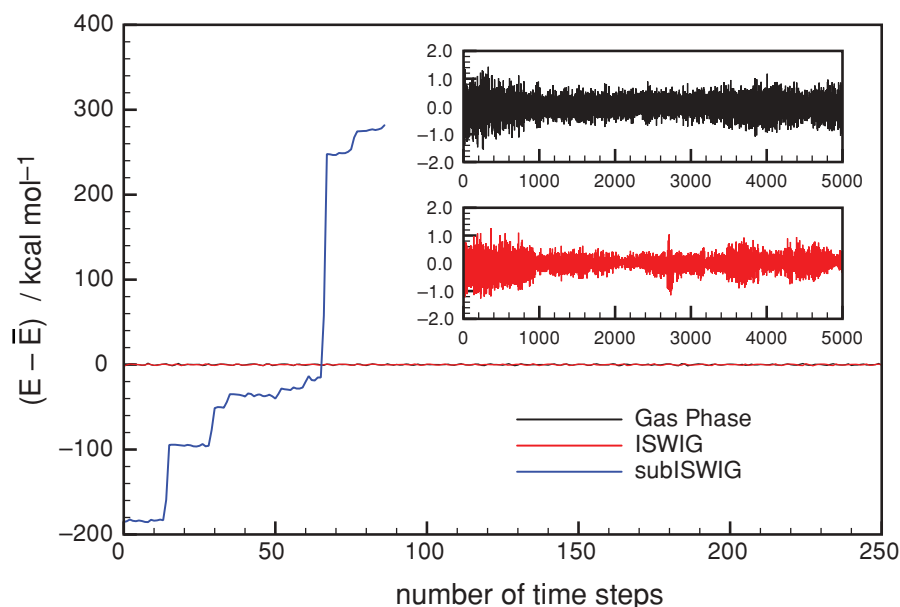


FIG. 9. Fluctuations in the energy during an MD simulation of glycine in water, described at the PBE0/6-31+G*/SS(V)PE level. The inset shows a close-up view of the energy fluctuations obtained in the gas phase and with SS(V)PE[ISWIG] over the entire simulation. The time step is 0.97 fs.

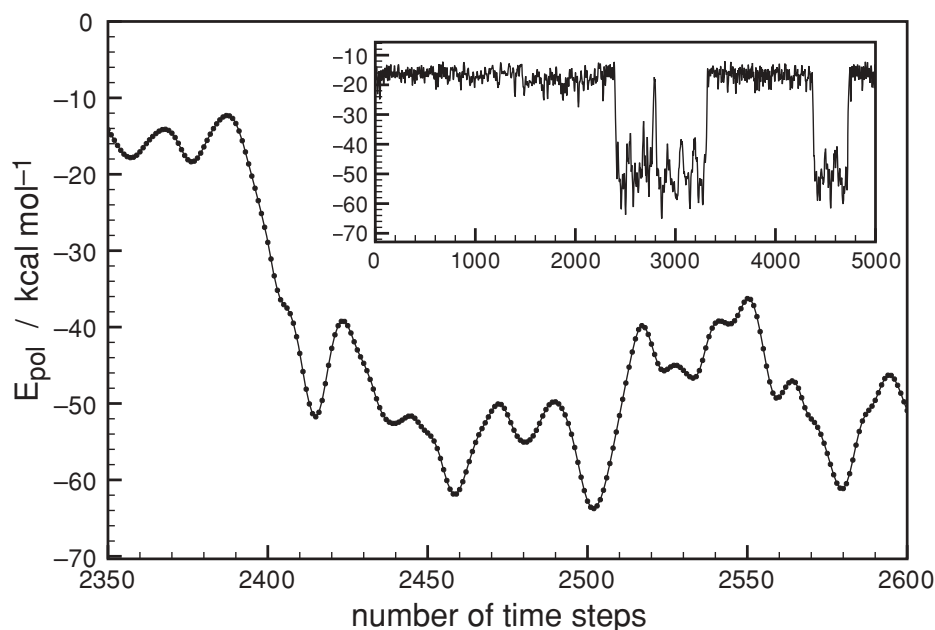


FIG. 10. Solvation energy, E_{pol} , of glycine in water, during an MD simulation performed at the PBE0/6-31+G*/SS(V)PE[ISWIG] level. The regions around -15 kcal/mol represent the carboxylic acid tautomer, whereas lower-energy regions (around -50 kcal/mol) represent the zwitterion. The inset shows a longer amount of simulation time, and indicates that proton transfer occurs multiple times. The time step in this simulation is 0.97 fs.

ACKNOWLEDGMENTS

This work was supported by an NSF CAREER award (CHE-0748448). Calculations were performed at the Ohio Supercomputer Center (Project No. PAS-0291). J.M.H. is an Alfred P. Sloan Foundation fellow.

APPENDIX A: INTEGRAL EQUATION FORMULATION

Here, we show how different PCMs are represented in the context of the reaction-field equations presented in Sec. II. The relevant integral operators are described in detail elsewhere.^{2,3,8} Briefly, the operator \hat{S} acts on an arbitrary surface charge density, $\sigma(\vec{s})$, to generate the corresponding electrostatic potential on the surface:

$$\hat{S}\sigma(\vec{s}) = \int \frac{\sigma(\vec{s}')}{|\vec{s} - \vec{s}'|} d^2\vec{s}' = \phi(\vec{s}). \quad (\text{A1})$$

The operator \hat{D}^\dagger acts on $\sigma(\vec{s})$ to produce the negative of the normal component of the electric field,

$$\begin{aligned} \hat{D}^\dagger\sigma(\vec{s}) &= \int \sigma(\vec{s}') \frac{\vec{n}_s \cdot (\vec{s} - \vec{s}')}{|\vec{s} - \vec{s}'|^3} d^2\vec{s}' \\ &= -\vec{F}(\vec{s}) \cdot \vec{n}_s. \end{aligned} \quad (\text{A2})$$

(Here, \vec{n}_s is the outward-pointing unit vector normal to the cavity surface, at the point \vec{s} .) We also define \hat{D} , the adjoint of \hat{D}^\dagger , and note that

$$\hat{D}\hat{S} = \hat{S}\hat{D}^\dagger. \quad (\text{A3})$$

As noted in Sec. II C 3, however, this equality is generally *not* preserved when these operators are discretized to yield finite-dimensional matrices.^{2,57}

In Sec. II A we introduced w_{displ} , the work required to displace the bound charges within the dielectric. Our goal here is to obtain an expression for this quantity, in terms of the electrostatic interactions at the cavity surface. Various PCMs afford different expressions for w_{displ} , and although the original derivations of these models did not explicitly invoke the charge-displacement work, we will show that all of them can be recast into the framework of Eq. (2.10), whence an expression for w_{displ} is obtained.

The simplest possible continuum model is obtained by assuming that the medium is a conductor. In this case, $w_{\text{displ}} = 0$ because charges in the continuum are unbound. Expressions for w_{displ} in finite-dielectric models are not as obvious but can be obtained after some algebra. The resulting expressions for w_{displ} in C-PCM and SS(V)PE are given in Table VI. Note that in each case, $w_{\text{displ}} \rightarrow 0$ as $\epsilon \rightarrow \infty$.

As a check of these expressions for w_{displ} , we insert them into the variational condition, Eq. (2.13). Upon rearranging the result, one obtains the condition

$$\hat{S}\sigma_{\text{pol}}(\vec{s}) = -\left(\frac{\epsilon - 1}{\epsilon}\right)\phi_0(\vec{s}) \quad (\text{A4})$$

TABLE VI. Definitions of w_{displ} for various continuum models. The quantity ϵ represents the dielectric constant of the medium.

Continuum Model	w_{displ}
Conductor	0
C-PCM	$\frac{1}{2} \left(\frac{1}{\epsilon - 1}\right) \int \sigma_{\text{pol}}(\vec{s}) \hat{S}\sigma_{\text{pol}}(\vec{s}) d^2\vec{s}$
SS(V)PE	$\left(\frac{1}{\epsilon - 1}\right) \int \sigma_{\text{pol}}(\vec{s}) \left[\hat{I} - \frac{1}{2\pi} \hat{D}\right]^{-1} \hat{S}\sigma_{\text{pol}}(\vec{s}) d^2\vec{s}$

in the case of C-PCM, whereas for SS(V)PE, the variational condition can be written

$$\begin{aligned} & \left[\hat{I} - \left(\frac{\varepsilon - 1}{\varepsilon + 1} \right) \frac{1}{2\pi} \hat{D} \right] \hat{S}\sigma_{\text{pol}}(\vec{s}) \\ &= - \left(\frac{\varepsilon - 1}{\varepsilon + 1} \right) \left[\hat{I} - \frac{1}{2\pi} \hat{D} \right] \phi_0(\vec{s}). \end{aligned} \quad (\text{A5})$$

These two equations are precisely the standard PCM working equations for these two models, which can be expressed in the general form²⁻⁴ [cf. Eq. (2.18)]

$$\hat{K}\sigma_{\text{pol}}(\vec{s}) = \hat{R}\phi_0(\vec{s}). \quad (\text{A6})$$

Discretization of Eqs. (A4) and (A5) affords the matrix forms of \mathbf{K} and \mathbf{R} that appear in Table I. [Note the symmetrization that is performed in the SS(V)PE case, since $\mathbf{DAS} \neq \mathbf{SAD}^\dagger$.]

Defining $\hat{Q} = \hat{K}^{-1}\hat{R}$, it follows from Eqs. (2.15) and (A6) that

$$-\hat{Q}^{-1}\sigma_{\text{pol}}(\vec{s}) = \hat{S}\sigma_{\text{pol}}(\vec{s}) + \frac{\delta W_{\text{displ}}}{\delta \sigma_{\text{pol}}(\vec{s})}. \quad (\text{A7})$$

Invoking the condition that W should be minimized with respect to variation of σ_{pol} [Eq. (2.14)], it follows that the operator \hat{Q} must be negative-definite. (This same result was demonstrated, in a somewhat different fashion, in Ref. 57.)

APPENDIX B: CONTINUITY

Here we show how the switching function in SWIG and similar methods ensures that the solute's potential energy surface is continuous. Our proof generalizes the one given in Ref. 16 for the YK version of COSMO.

We begin by decomposing the \mathbf{K} matrix from Eq. (2.18) into a sum of its diagonal and off-diagonal contributions, $\mathbf{K} = \mathbf{K}_{\text{diag}} + \mathbf{K}_{\text{off}}$. We can then express \mathbf{K} as

$$\mathbf{K} = \mathbf{K}_{\text{diag}}^{1/2} \mathbf{L} \mathbf{K}_{\text{diag}}^{1/2}, \quad (\text{B1})$$

where

$$\mathbf{L} = \mathbf{I} + \mathbf{K}_{\text{diag}}^{-1/2} \mathbf{K}_{\text{off}} \mathbf{K}_{\text{diag}}^{-1/2} \quad (\text{B2})$$

and \mathbf{I} is a unit matrix. Inserting Eq. (B1) into Eq. (2.20), one may express the solvation energy as

$$E_{\text{pol}} = \frac{1}{2} \mathbf{v}^\dagger \mathbf{K}_{\text{diag}}^{-1/2} \mathbf{L}^{-1} \mathbf{K}_{\text{diag}}^{1/2} \mathbf{y}, \quad (\text{B3})$$

where $\mathbf{y} = \mathbf{R}\mathbf{v}$.

The key point is that every term in the diagonal matrix element K_{ii} contains a factor of S_{ii} , for each of the solvation models considered here (see Table I.) Thus, by placing the switching function F_i in the denominator of S_{ii} [Eq. (3.7)], we ensure that the i th diagonal element of $\mathbf{K}_{\text{diag}}^{-1/2}$ goes to zero as $F_i \rightarrow 0$. For the FIXPVA and CSC methods, $a_i \rightarrow 0$ as \vec{s}_i enters the cavity, which has the same effect, according to Eq. (4.1).

It then follows from Eqs. (B1) and (B2) that \mathbf{K}^{-1} has a null space corresponding to those surface elements for which $F_i = 0$, and that \mathbf{L} acts as a unit matrix within this null space. As such, the dimension of $\mathbf{q} = \mathbf{K}^{-1}\mathbf{y}$ can be reduced *without approximation* to include only those surface grid points for

which $F_i > 0$. For the same reason, the i th grid point's contribution to E_{pol} vanishes as $F_i \rightarrow 0$. Since F_i is a smooth function of the nuclear coordinates, so is E_{pol} .

APPENDIX C: SWITCHING FUNCTION GRADIENT

The gradient of the switching function F_i with respect to the M th solute nucleus is

$$\hat{\nabla}_M F_i = F_i \sum_J^{\text{atoms}} \frac{\hat{\nabla}_M f(\vec{s}_i, \vec{r}_J)}{f(\vec{s}_i, \vec{r}_J)}. \quad (\text{C1})$$

For the elementary switching function $f(\vec{s}_i, \vec{r}_J)$ that is defined in Eq. (3.18), the derivative with respect to a perturbation of the M th nucleus is

$$\hat{\nabla}_M f(\vec{s}_i, \vec{r}_J) = \frac{\partial h(d_{iJ})}{\partial d_{iJ}} \hat{\nabla}_M d_{iJ}. \quad (\text{C2})$$

The derivative $\partial h(d_{iJ})/\partial d_{iJ}$ is easily derived from Eq. (3.19), while the other term in Eq. (C2) is given by

$$\hat{\nabla}_M d_{iJ} = \left(\frac{\vec{r}_i - \vec{r}_J}{r_{iJ}} \right) \frac{\delta_{iM} - \delta_{JM}}{R_{sw,J}}. \quad (\text{C3})$$

For the alternative elementary switching function defined in Eq. (3.20), the gradient is

$$\hat{\nabla}_M f(\vec{s}_i, \vec{r}_J) = \frac{\partial f(\vec{r}_i, \vec{r}_J)}{\partial r_{iJ}} \hat{\nabla}_M r_{iJ}, \quad (\text{C4})$$

where

$$\begin{aligned} \frac{\partial f(\vec{s}_i, \vec{r}_J)}{\partial r_{iJ}} &= \frac{\zeta_i}{\sqrt{\pi}} \left\{ \exp[-\zeta_i^2 (R_J - r_{iJ})^2] \right. \\ &\quad \left. + \exp[-\zeta_i^2 (R_J + r_{iJ})^2] \right\} \end{aligned} \quad (\text{C5})$$

and

$$\hat{\nabla}_M r_{iJ} = \frac{\vec{r}_J - \vec{s}_i}{r_{iJ}} (\delta_{JM} - \delta_{iM}). \quad (\text{C6})$$

For Lebedev discretization, the i th quadrature point contributes $a_i = w_i R_J^2 F_i$ to the total surface area. From Eq. (C1), it follows that

$$\hat{\nabla}_M a_i = a_i \sum_J^{\text{atoms}} \frac{\hat{\nabla}_M f(\vec{s}_i, \vec{r}_J)}{f(\vec{s}_i, \vec{r}_J)}. \quad (\text{C7})$$

In view of this result, the expression for the gradient of the total cavity surface area is considerably simpler than it is in either the GEPOL surface tessellation approach³² or the FIXPVA method.²⁰ Although we do not consider nonelectrostatic solute–continuum interactions in the present work, Eq. (C7) shows that the SWIG approach leads to simple expressions for the gradients of typical nonelectrostatic interaction terms,^{22,23} which are explicit functions of the cavity surface area.

¹J. Tomasi, B. Mennucci, and R. Cammi, *Chem. Rev.* **105**, 2999 (2005).

²D. M. Chipman, *Theor. Chem. Acc.* **107**, 80 (2002).

³D. M. Chipman, *J. Chem. Phys.* **112**, 5558 (2000).

⁴D. M. Chipman and M. Dupuis, *Theor. Chem. Acc.* **107**, 90 (2002).

⁵V. Barone and M. Cossi, *J. Phys. Chem. A* **102**, 1995 (1998).

⁶T. N. Truong and E. V. Stefanovich, *Chem. Phys. Lett.* **240**, 253 (1995).

⁷T. N. Truong, U. N. Nguyen, and E. V. Stefanovich, *Int. J. Quantum Chem. Symp.* **30**, 1615 (1996).

- ⁸E. Cancès, B. Mennucci, and J. Tomasi, *J. Chem. Phys.* **107**, 3032 (1997).
- ⁹B. Mennucci, E. Cancès, and J. Tomasi, *J. Phys. Chem. B* **101**, 10506 (1997).
- ¹⁰J. Tomasi, B. Mennucci, and E. Cancès, *J. Mol. Struct.: THEOCHEM* **464**, 211 (1999).
- ¹¹E. Cancès and B. Mennucci, *J. Chem. Phys.* **114**, 4744 (2001).
- ¹²J. B. Foresman, T. A. Keith, K. B. Wiberg, J. Snoonian, and M. J. Frisch, *J. Phys. Chem.* **100**, 16098 (1996).
- ¹³V. Barone, M. Cossi, and J. Tomasi, *J. Chem. Phys.* **107**, 3210 (1997).
- ¹⁴B. Ginovska, D. M. Camaioni, M. Dupuis, C. A. Schwerdtfeger, and Q. Gil, *J. Phys. Chem. A* **112**, 10604 (2008).
- ¹⁵A. W. Lange and J. M. Herbert, *J. Phys. Chem. Lett.* **1**, 556 (2010).
- ¹⁶D. M. York and M. Karplus, *J. Phys. Chem. A* **103**, 11060 (1999).
- ¹⁷A. Klamt and G. Schüürmann, *J. Chem. Soc. Perkin Trans. 2*, 799 (1993).
- ¹⁸C. S. Pomelli, *J. Comput. Chem.* **25**, 1532 (2004).
- ¹⁹H. Li and J. H. Jensen, *J. Comput. Chem.* **25**, 1449 (2004).
- ²⁰P. Su and H. Li, *J. Chem. Phys.* **130**, 074109 (2009).
- ²¹G. Scalmani and M. J. Frisch, *J. Chem. Phys.* **132**, 114110 (2010).
- ²²F. M. Floris, J. Tomasi, and J. L. Pascual-Ahuir, *J. Comput. Chem.* **12**, 784 (1991).
- ²³M. Cossi, V. Barone, R. Cammi, and J. Tomasi, *Chem. Phys. Lett.* **255**, 327 (1996).
- ²⁴L. Onsager, *J. Am. Chem. Soc.* **58**, 1486 (1936).
- ²⁵J. G. Kirkwood, *J. Chem. Phys.* **2**, 351 (1934).
- ²⁶M. Born, *Z. Phys.* **1**, 45 (1920).
- ²⁷A. Bondi, *J. Phys. Chem.* **68**, 441 (1964).
- ²⁸R. Bonaccorsi, P. Palla, and J. Tomasi, *J. Am. Chem. Soc.* **106**, 1945 (1984).
- ²⁹M. L. Connolly, *J. Appl. Crystallog.* **16**, 548 (1983).
- ³⁰J. L. Pascual-Ahuir, E. Silla, and I. Tunon, *J. Comput. Chem.* **15**, 1127 (1994).
- ³¹V. I. Lebedev, *USSR Comp. Math. Math+* **15**, 44 (1975).
- ³²M. Cossi, B. Mennucci, and R. Cammi, *J. Comput. Chem.* **17**, 57 (1996).
- ³³G. Scalmani, V. Barone, K. N. Kudin, C. S. Pomelli, G. E. Scuseria, and M. J. Frisch, *Theor. Chem. Acc.* **111**, 90 (2004).
- ³⁴R. Cammi and J. Tomasi, *J. Chem. Phys.* **100**, 7495 (1994).
- ³⁵R. Cammi and J. Tomasi, *J. Chem. Phys.* **101**, 3888 (1994).
- ³⁶E. Cancès, B. Mennucci, and J. Tomasi, *J. Chem. Phys.* **109**, 260 (1998).
- ³⁷M. Cossi, G. Scalmani, N. Rega, and V. Barone, *J. Chem. Phys.* **117**, 43 (2002).
- ³⁸M. Cossi, N. Rega, G. Scalmani, and V. Barone, *J. Comput. Chem.* **24**, 669 (2002).
- ³⁹J. A. Pople, R. Krishnan, H. B. Schegel, and J. S. Binkley, *Int. J. Quantum Chem. Symp.* **13**, 225 (1979).
- ⁴⁰F. Chen and D. M. Chipman, *J. Chem. Phys.* **119**, 10289 (2003).
- ⁴¹B. A. Gregersen and D. M. York, *J. Chem. Phys.* **122**, 194110 (2005).
- ⁴²See supplementary material at <http://dx.doi.org/10.1063/1.3511297> for definitions of the switching function parameters and numerical data regarding convergence with respect to the number of Lebedev grid points.
- ⁴³J. Khandogin, B. A. Gregersen, W. Thiel, and D. M. York, *J. Phys. Chem. B* **109**, 9799 (2005).
- ⁴⁴D. M. Chipman, *J. Chem. Phys.* **110**, 8012 (1999).
- ⁴⁵A. Rashin and K. Namboodiri, *J. Phys. Chem.* **91**, 6003 (1987).
- ⁴⁶E. O. Purisima and S. H. Nilar, *J. Comput. Chem.* **16**, 681 (1995).
- ⁴⁷Y. Shao, L. Fusti-Molnar, Y. Jung, J. Kussmann, C. Ochsenfeld, S. T. Brown, A. T. B. Gilbert, L. V. Slipchenko, S. V. Levchenko, D. P. O'Neill, R. A. DiStasio, Jr, R. C. Lochan, T. Wang, G. J. O. Beran, N. A. Besley, J. M. Herbert, C. Y. Lin, T. Van Voorhis, S. H. Chien, A. Sodt, R. P. Steele, V. A. Rassolov, P. E. Maslen, P. P. Korambath, R. D. Adamson B. Austin, J. Baker, E. F. C. Byrd, H. Dachsel, R. J. Doerksen, A. Dreuw, B. D. Dunietz, A. D. Dutoi, T. R. Furlani, S. R. Gwaltney, A. Heyden, S. Hirata, C.-P. Hsu, G. Kedziora, R. Z. Khalliulin, P. Klunzinger, A. M. Lee, M. S. Lee, W. Liang, I. Lotan, N. Nair, B. Peters, E. I. Proynov, P. A. Pieniazek, Y. M. Rhee, J. Ritchie, E. Rosta, C. D. Sherrill, A. C. Simmonett, J. E. Subotnik, H. L. Woodcock III, W. Zhang, A. T. Bell, A. K. Chakraborty, D. M. Chipman, F. J. Keil, A. Warshel, W. J. Hehre, H. F. Schaefer III, J. Kong, A. I. Krylov, P. M. W. Gill, and M. Head-Gordon, *Phys. Chem. Chem. Phys.* **8**, 3172 (2006).
- ⁴⁸R. S. Rowland and R. Taylor, *J. Phys. Chem.* **100**, 7384 (1996).
- ⁴⁹J. Wang, P. Cieplak, and P. A. Kollman, *J. Comput. Chem.* **21**, 1049 (2000).
- ⁵⁰One could reasonably argue that the use of AMBER99 point charges is inappropriate for bond-breaking, and that ionic radii for Na⁺ and Cl⁻ should not be used when the Na-Cl distance is small. However, our intention here is not to develop an accurate model of bond-breaking in solution, but rather to explore the singularities that can occur as atomic spheres interpenetrate, and this simple example suffices for that purpose.
- ⁵¹A. Klamt, B. Mennucci, J. Tomasi, V. Barone, C. Curutchet, M. Orozco, and F. J. Luque, *Acc. Chem. Res.* **42**, 489 (2009).
- ⁵²In test calculations using the Adaptive Poisson-Boltzmann Solver, (Ref. 53), we observed deviations of < 0.1 kcal/mol in the solvation energies of randomly selected rotations of alanine, even using coarse grids with $\Delta x = 0.3$ Å for which solvation energies are certainly not converged.
- ⁵³N. A. Baker, D. Sept, S. Joseph, M. J. Holst, and J. A. McCammon, *Proc. Natl. Acad. Sci. U.S.A.* **98**, 10037 (2001).
- ⁵⁴TINKER, version 4.2, <http://dasher.wustl.edu/tinker>.
- ⁵⁵J. H. Jensen and M. S. Gordon, *J. Am. Chem. Soc.* **117**, 8159 (1995).
- ⁵⁶P. Bandyopadhyay, M. S. Gordon, B. Mennucci, and J. Tomasi, *J. Chem. Phys.* **116**, 5023 (2002).
- ⁵⁷F. Lipparini, G. Scalmani, B. Mennucci, E. Cancès, M. Caricato, and M. J. Frisch, *J. Chem. Phys.* **133**, 014106 (2010).